AFIT/GAP/ENP/93D-05

CHARACTERIZATION OF AN LCD FOR USE AS A PROGRAMMABLE PHASE SHIFTER TO PRODUCE A SINGLE-LOBED FAR-FIELD PATTERN IN A PHASED ARRAY

THESIS

Gregory S. Kenyon, Captain, USAF

AFIT/GAP/ENP/93D-05

AFIT/GAP/ENP/93D-05

CHARACTERIZATION OF AN LCD FOR USE AS A PROGRAMMABLE PHASE SHIFTER TO PRODUCE A SINGLE-LOBED FAR-FIELD PATTERN IN A PHASED ARRAY

THESIS

Presented to the Faculty of the School of Engineering
of the Air Force Institute of Technology
Air University
in Partial Fulfillment of the
Requirements for the Degree of
Master of Science in Engineering Physics

Gregory S. Kenyon, B.S.
Captain, USAF

December 1993

ACKNOWLEDGEMENTS

"Thanks be to God for his indescribable gift!"

2 Corinthians 9:15 (NIV).

I wish to thank my wife, Cathy, and my daughter, Chelsea, for their many sacrifices, and my parents for their continuing support and encouragement. I greatly appreciate my advisor Dr. Won B. Roh, and the members of my committee, Maj. Glen Perram and Capt. Jeff Grantham for sharing their great expertise with me.

I also wish to thank the following people for making this project possible: Nancy Ashworth-Loy, Capt. Roy Calfas, Leroy Cannon, Karen Dobbyn, Bill Evans, Capt. Rob Franklin, Lt. Mike Hawks, Diana Jordan, Capt. Alan Ratcliff, Jim Reynolds, Capt. Mike Roggemann, Greg Smith, and Capt. Greg Vansuch.

Gregory S. Kenyon

TABLE OF CONTENTS

LIST OF FIGURES

ABSTRACT

The liquid crystal display (LCD) from an inexpensive pocket television was converted to a spatial light modulator (SLM) for the purpose of altering the phase front of a ten element diode laser array to produce a single lobe far field pattern. Characterization of the SLM determined the amount of phase shift, amplitude modulation and polarization rotation properties. Nonuniformities within the phase shifter and insufficient phase shift prevented the formation of a single lobe. However, a very limited phase grating was created and analyzed. LCDs from inexpensive commercial pocket televisions were found unsuitable for use as phase shifting spatial light modulators.

I. INTRODUCTION

Phased diode laser arrays are very efficient at producing high power coherent beams for a variety of applications. Unfortunately arrays, composed of similar elements, operate in an array mode in which successive elements are 180^0 out of phase, producing a double-lobed intensity pattern in the far field.[1] A variety of techniques to produce a single lobe have been investigated.[1-9] All of these techniques have limitations in their effectiveness and/or their ability to be used in a military/commercial application. Previous researchers have been partially successful in producing a single lobe, by altering the wave front with a fixed phase shifter. The purpose of this research project was to develop and demonstrate a technique, using a programmable phase shifter, that would enable future researchers to determine an optimum phase shift which could then be incorporated into a production feasible system.

The phase shifter in this experiment was the modified liquid crystal display (LCD) from an inexpensive pocket television. Prior to phase shifting experiments, the LCD was characterized to determine the amount of phase shift, amplitude modulation and polarization rotation properties. The maximum possible phase shift was determined by placing it in a Mach-Zehnder interferometer. The ability of the phase shifter, to shift different sections of a laser array output by varying amounts, was determined by creating and analyzing a phase grating. The

grating diffracted power from the central lobe of the laser into side lobes. The amount of peak to peak phase shift in the grating was determined by measuring a decrease in power in the central lobe as the strength of the grating was increased.

The LCD's ability to modulate amplitude was determined by simply measuring the variations in the transmitted power. Polarization rotation properties were determined by measuring the change in the power transmission through the phase shifter and an analyzing polarizer, as the orientation of the polarizer was varied.

The LCD was found to be capable of producing a maximum phase shift of approximately 30% to 60% of a wave. The programmable difference in phase shift, from one pixel of the display to the next, was on the order of a few percent of a wave. Even as slight a phase shift as this would have helped to move a small amount of power into the center of the radiation pattern. However, nonuniformities across the LCD diffracted a large amount of power away from the central lobe and would have eliminated any small benefit from altering the phase front of the array. It is for these reasons that LCDs from inexpensive commercial pocket televisions were judged unsuitable for use as phase shifting spatial light modulators.

II. THEORY/BACKGROUND

Individual elements in a diode laser array behave in a manner similar to a single laser. However, because of an overlap in their electromagnetic fields, these elements influence each other in such a way that the array may only operate in certain distinct array modes. For instance, all of the elements could lase in-phase or adjacent elements could lase 180^0 out-of-phase as shown in Figure 1.[10] In the in-phase mode the EM fields of the individual elements would add to produce significant fields in the lossy region between the elements causing larger losses for this mode. In the out-of-phase mode, the fields would have a null in the region between elements so this mode has much lower losses and tends to be the mode in which diode laser arrays operate.

For an array with an even number of elements operating in the in-phase mode, the combined wave front may be approximated by a full-rectified sine function times a Gaussian function. Where a Gaussian function may be written as

$$Gaus\left(\frac{x-x_o}{b}\right) = \exp\left[-\pi\left(\frac{x-x_o}{b}\right)^2\right]. \qquad (1)$$

For the out-of-phase array mode, the combined wave front may be approximated by a sine function modulated by a Gaussian function. Examples of these two approximate solutions to the array near field modes may be seen in Figure 2. Scalar diffraction theory predicts that in the far field or Fraunhofer region the field

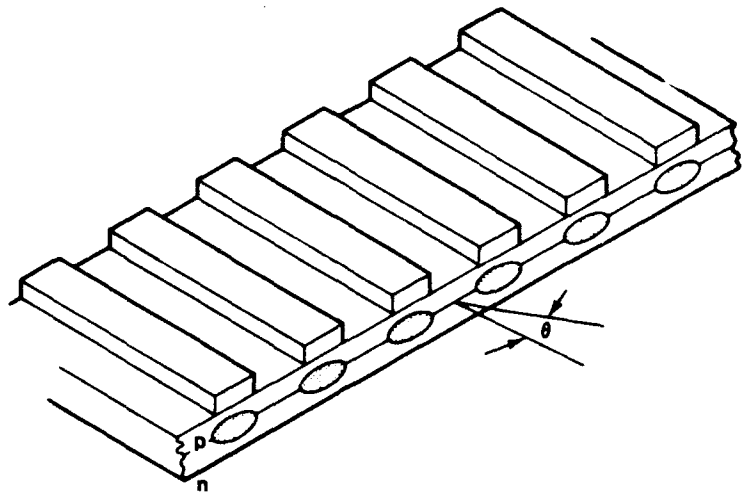

(a) A typical 6-stripe semiconductor array.

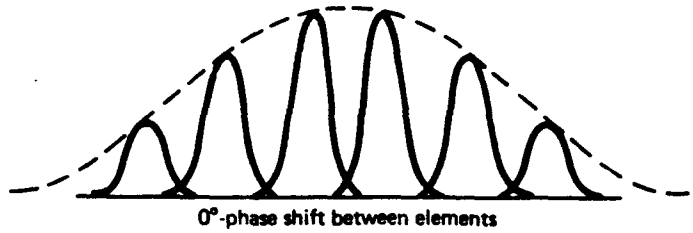

(b) An in-phase field distribution.

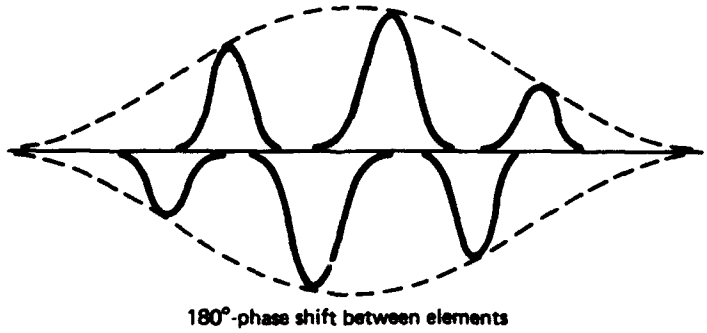

(c) The same field elements as (b) but with a 180° phase shift between adjacent stripes.

Figure 1. Array Near Field Radiation Pattern (From Reference 10)

$$\left|\sin(x)\right| \cdot \mathrm{Gaus}\left(\frac{x}{10}\right)$$

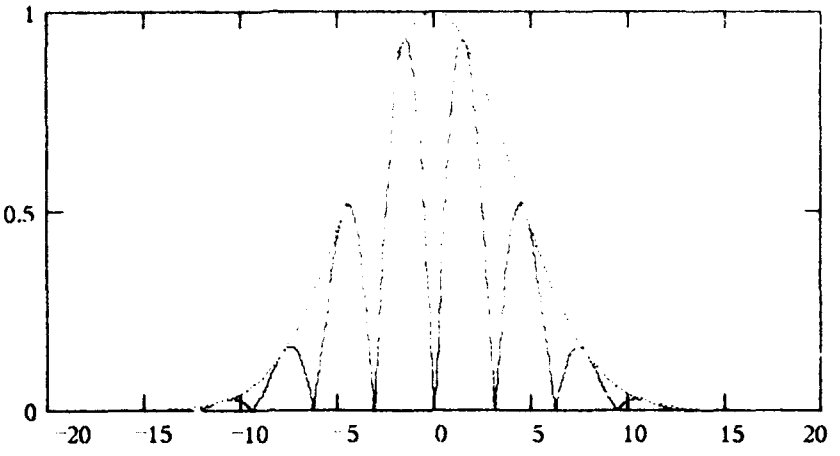

$$\sin(x) \cdot \mathrm{Gaus}\left(\frac{x}{10}\right)$$

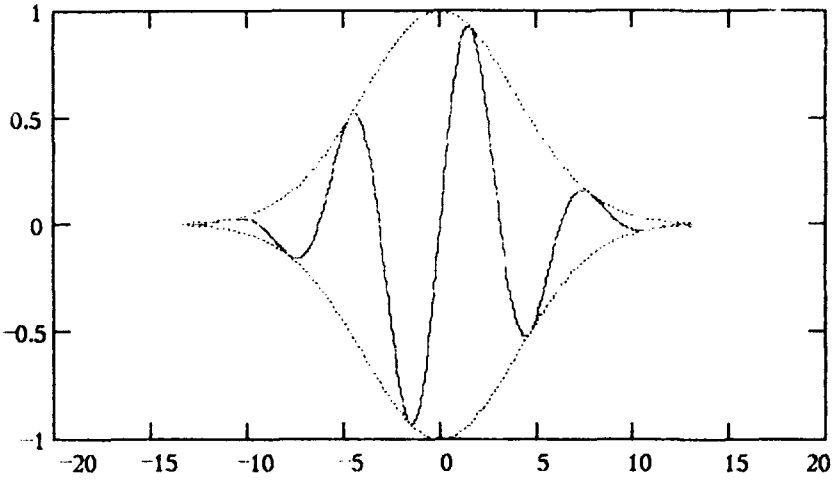

Figure 2. Approximate Array Near Field Radiation Pattern

distribution should simply be the Fourier transform of the original field distribution.[11] The Fourier transform of a rectified sine function (calculated in Appendix A) has a main central lobe with much smaller side lobes, as can be seen in Figure 3. The Fourier transform of a sine multiplied by a Gaussian is a pair of displaced Gaussian functions (calculated in Appendix B), as can be seen in Figure 4. This explains the production of the single and double lobe intensity patterns for the in-phase and out-of-phase modes.

Many applications of diode laser arrays require a large amount of power concentrated in a small area. For this reason several techniques have been used to eliminate the double-lobed pattern. In one of these, the arrays have been placed in external cavities containing spatial filters to force the array into the in-phase mode.[2] A phase-conjugate mirror has also been used to phase-conjugate one of the lobes forcing the array to operate with a single lobe.[3]

Another technique allows the array to run in the out-of-phase mode and then rectifies the near field radiation pattern using phase shifters. The near field has been rectified by using internal phase shifters on every other element.[1] The elements would operate in the out-of-phase mode for most of their length producing favorable gain characteristics. The internal phase shifter, placed near the emitting facet, would make the array appear to be in the in-phase mode.

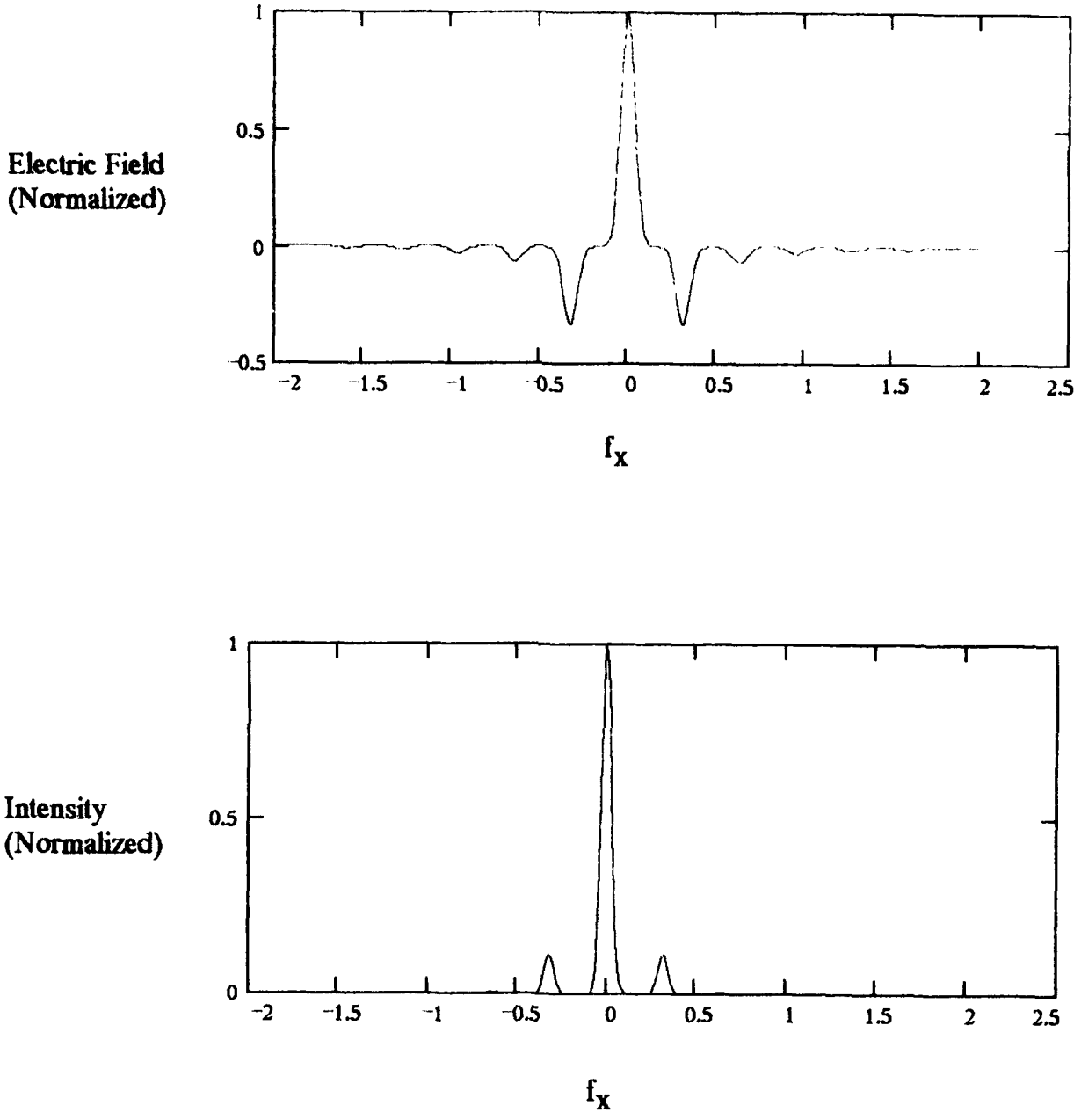

Figure 3. Electric Field (Top) and Intensity Pattern (Bottom) in the Far Field for In-Phase Mode Near Field

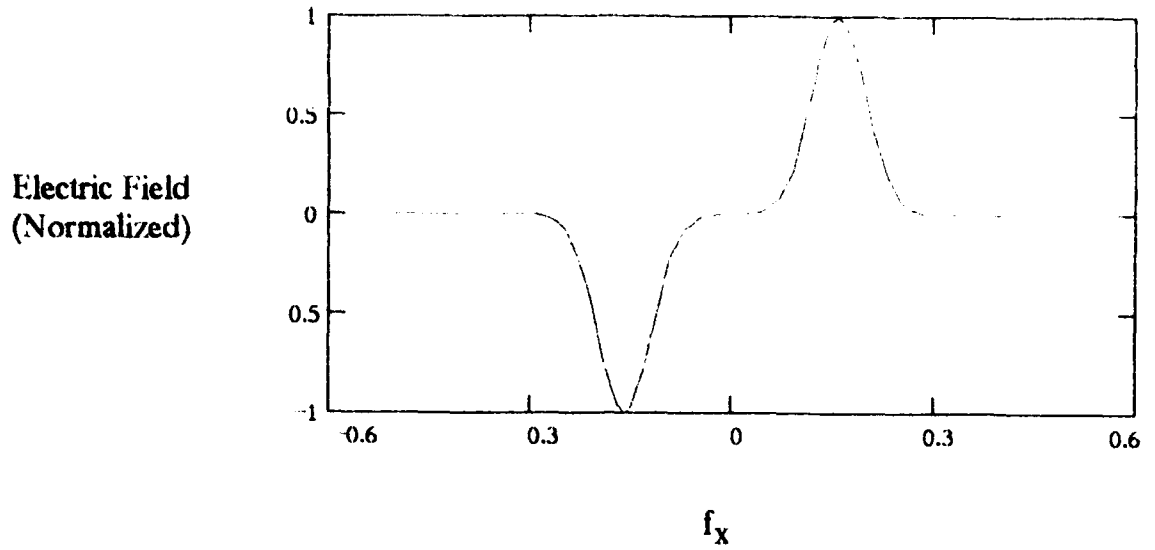

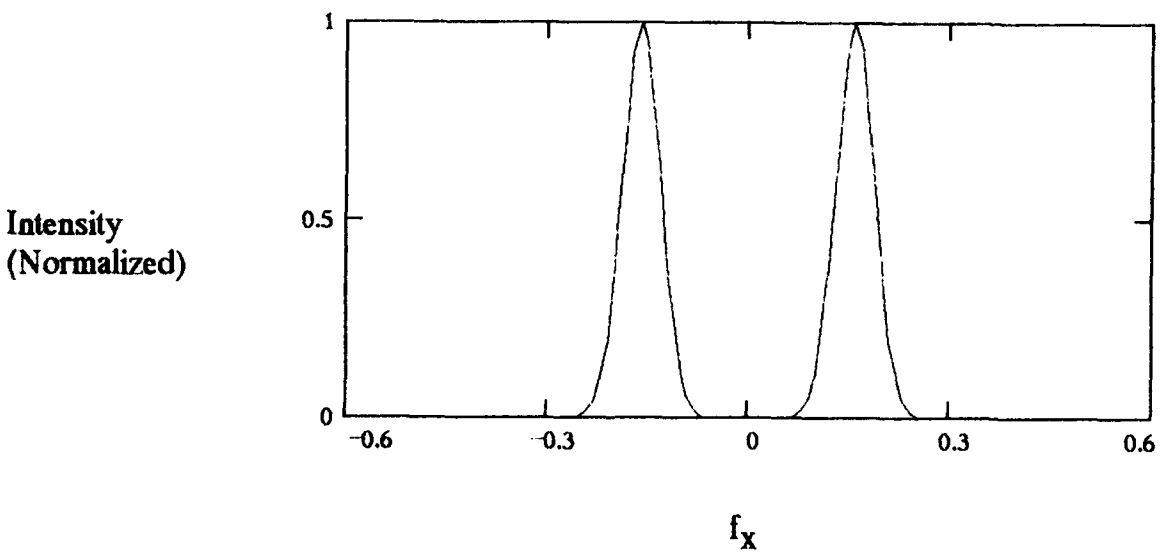

Figure 4. Electric Field (Top) and Intensity Pattern (Bottom) in the Far Field for the Out-of-Phase Mode Near Field

A variety of external phase shifters have also been used. Fixed phase shifters, either near contact phase shifters[4] or shifters integrated with the array[5], were made by etching a pattern into a semiconducting material, using the index difference between air and the etched material to create the index grating. A variable external phase shifter may be created by using an amplifier with several elements.[6,7] By varying the injection current to individual elements, the index of refraction, and hence the phase shift of each element was varied.

Several other methods have also been used to help create a single spot. Anamorphic prism optics have been used to focus the light from the two lobes down into a single circular spot.[8] An algorithm has been proposed for the selection of certain elements in large arrays.[9] Elements that helped in producing a single spot would be turned on while elements that dispersed the light would be turned off.

The technique used in this experiment was to use an inexpensive programmable spatial phase modulator (SPM) for rectifying the phase front. The SPM chosen for the present experiment was the liquid crystal display (LCD) of a pocket television set. The display is made of a twisted nematic liquid-crystal cell. The cell contains a thin layer of liquid crystal material sandwiched between two glass plates containing transparent conducting electrode patterns.[12] The liquid crystal material is composed of long, thread-like molecules that give the material a positive dielectric anisotropy. In a twisted nematic

liquid crystal cell, the glass plates are treated so that the liquid crystal material near the plate has homogeneous unidirectional alignment. The plates have alignment directions orthogonal to each other giving each layer in the cell a slight skew from the preceding layer. Each layer acts as a birefringent sheet rotating the polarization of light a total of 90^0 as it passes through the cell.

When a voltage is applied across the electrodes the liquid crystal molecules tend to realign parallel to the applied field.[13] If the voltage is lower than the optical threshold the molecules will tilt while maintaining their twisted orientation. Varying this voltage, and the corresponding tilt, will alter the index of refraction while maintaining the polarization rotation. A twisted nematic liquid crystal cell, operating below the optical threshold, placed between crossed polarizers will act as a phase modulator. By controlling the voltage of each pixel the index of refraction may be varied from one region to the next across the cell creating a spatial light modulator (SLM).

Liquid crystal cells (LCC) found in the liquid crystal displays of small pocket television sets are designed to operate as broadband amplitude modulators. An LCC is placed between parallel polarizers where it acts as a broadband polarization rotator similar to a Faraday cell. Very little intensity is transmitted at low applied voltages. The transmission increases with increasing applied voltage due to a loss in the polarization rotation properties in the LCC. The molecules in the LCC lose

their twist and simply tilt to align themselves with the increasing applied field.

The results of these two modes of operation, for a particular type of liquid crystal material (LC:E-7), can be seen in Figure 5. The liquid crystal cell used to gather the information in Figure 5 was from a single pixel cell. Therefore, the results from an experiment using an inexpensive multi-pixel cell may differ. Note the significant phase modulation below one and a half volts and the significant amplitude modulation above this voltage threshold. The vertical axis is in arbitrary units, however, the author notes that the phase change from peak to peak is equal to 2π.

It should be possible to create a phase modulating SLM by removing the secondary/analyzing polarizer from a LCD. The primary polarizer assures that the polarization of the light and the molecules in the liquid crystal cell are aligned. To get significant phase modulation the cell must be able to operate below the optical threshold. This approach formed the basis for the research described in the next chapter.

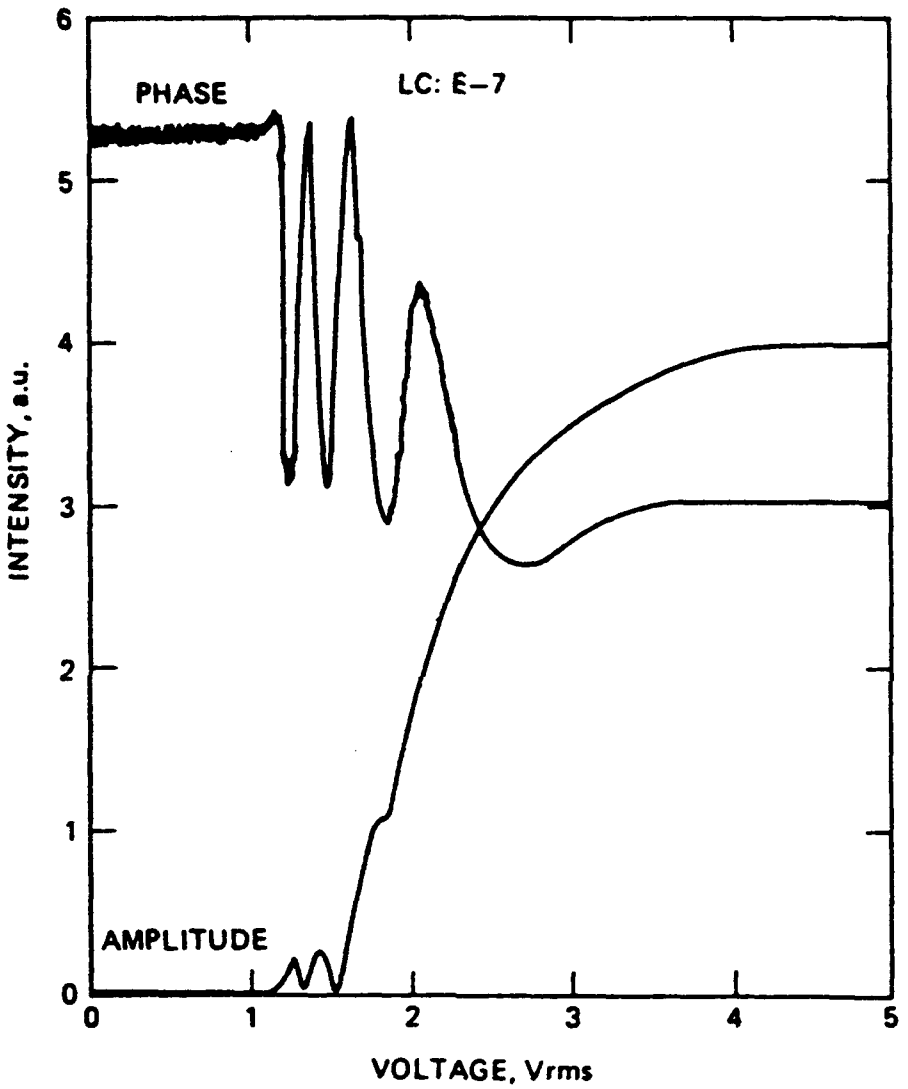

Figure 5. Phase Shift and Amplitude Modulation vs Applied Voltage (From Reference 13)

III. EXPERIMENT

The experiment was conducted in several steps. The first step was to characterize the phase shifting properties as a function of the DC bias voltage. The next step was to create and analyze a phase grating in the liquid crystal cell. The last step was to image the array near field onto the cell and then optimize the phase grating to produce a single lobe in the far field.

The liquid crystal cell used in this experiment was the display from a pocket television. Two cells were tested. One was a Realistic television (model number 16-161), the other was a Sharp LCD in a Sony television (model number FDL-370). The cell was controlled by the television with an input video signal from a black and white Cohu CCD video camera.

Characterization of Phase Shifter

Characterization of the phase shifter required knowing how the phase shift changed as the voltage across the liquid crystal cells was changed. The amplitude modulation characteristics of the SLM, between parallel polarizers, was also investigated. Characterization also included the confirmation of the phase shifter's ability to rotate polarization.

Amount of Phase Shift. The amount of phase shift was measured by placing the liquid crystal cell, with the primary polarizer, in one leg of a Mach-Zehnder interferometer as shown in Figure 6. To maintain a uniform applied voltage across the

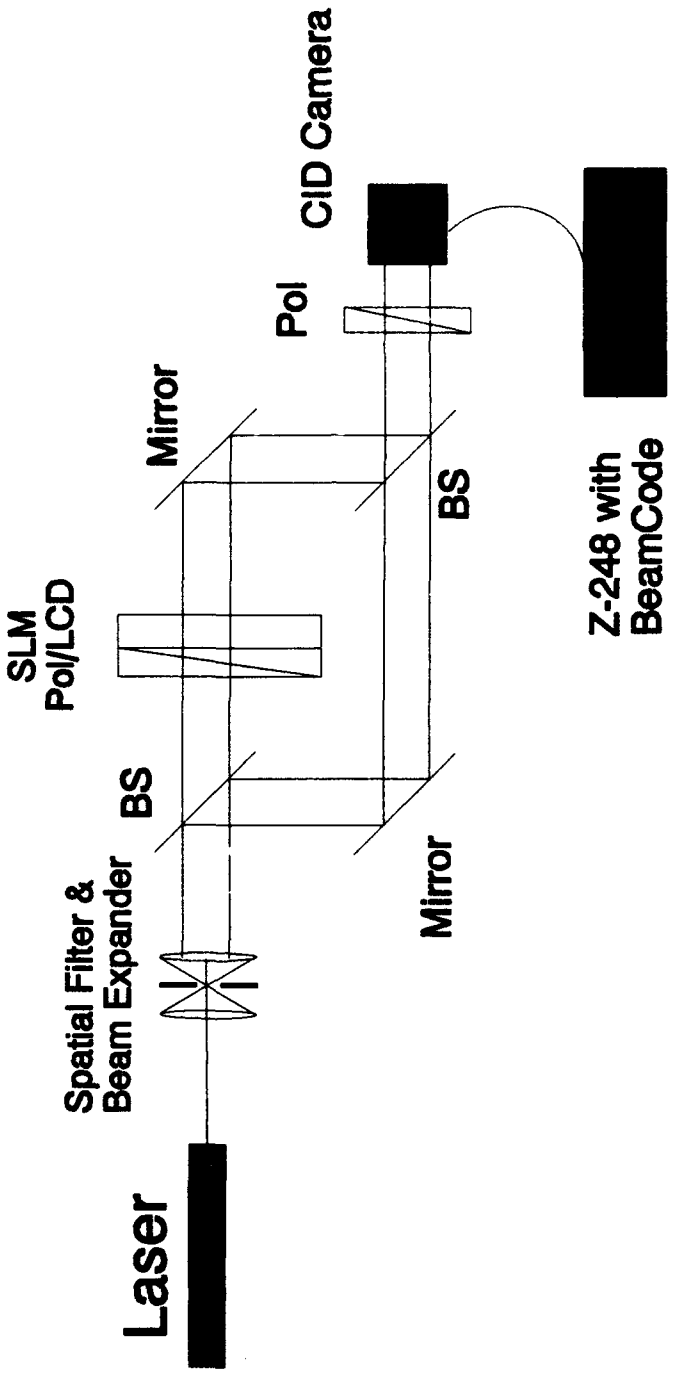

Figure 6. Mach-Zehnder Interferometer

cell, the lens cap was placed over the Cohu camera. The interference fringes were viewed using a GE CID camera connected to a Zenith 248 personal computer with BEAMCODE beam analysis software.

The orientation of the secondary polarizer was adjusted so that equal amounts of power from each leg of the interferometer were transmitted through the polarizer. Light from the LCD leg was polarized at 90^0 from the orientation of the manufacturer's primary polarizer. The polarization of light in the reference leg of the interferometer was controlled by the laser.

This experiment was performed with three different lasers, a HeNe, Argon ion and a GaAs single-mode diode laser. Depending on the power and polarization of the individual lasers, half wave plates were added as needed to the apparatus. To decrease the power, neutral density filters were occasionally added to the reference leg and in front of the camera. Each optical component degraded the fringe image quality so the fewest possible components were used.

The position of the interference fringes was recorded as the brightness control voltage was varied. The brightness control voltage is the voltage drop across the variable potentiometer that indirectly controls the image brightness of the original television. The image brightness of the Realistic television decreased with increasing brightness control voltage. However, the image brightness of the Sony television increased with

increasing brightness control voltage. Thus the arbitrary variable "brightness" was defined as in Equations 2 and 3.

$$Brightness = 1 - \frac{Voltage}{Maximum\ Voltage} \qquad (2)$$

for the Realistic TV set, and

$$Brightness = \frac{Voltage}{Maximum\ Voltage} \qquad (3)$$

for the Sony TV set,

where Voltage = Brightness Control Voltage.

Brightness was used as an indicator of the applied voltage across the cell since the actual applied voltage is controlled by a multiplexer and is inaccessible. The applied voltage should increase with increasing brightness.

The position of the fringes, at various brightness levels, provided both the distance that the fringes moved and the distance between fringes. The ratio of the fringe shift to the fringe separation distance was equal to the ratio of the phase shift, in radians, to 2π. This ratio was also the same as the fraction of a wave of phase shift.

The experiment was repeated, with the lens cap to the Cohu camera removed and a fixed brightness control voltage, while the strength of the TV signal was varied. The signal was varied by adjusting the aperture on the Cohu camera and by varying the illumination on a uniform test card used as the test object. The

strength of the signal was obtained by measuring the television video signal voltage on an oscilloscope.

Amplitude Modulation. To measure the amplitude modulation characteristics of the SLM, it was illuminated by a HeNe laser, as shown in Figure 7. A secondary analyzing polarizer was placed after the SLM. It was oriented for minimum transmission while the SLM was turned off. Thus, the polarizers were parallel to each other. The transmitted power was measured as the "Brightness" was varied.

Polarization Rotation. The previous apparatus was also used to confirm the polarization rotating properties of the SLM. The brightness was set to zero. Transmitted power was measured as the analyzing polarizer was rotated. The analyzing polarizer was then placed in front of the SLM and the experiment was repeated to determine the orientation of the manufacturer's polarizer.

Creation and Evaluation of Phase Grating

The phase grating was created by taking a picture of a striped test card (Figure 8) with the Cohu camera. The alignment of the phase grating was controlled by translating the camera from side to side. The periodicity of the phase grating was controlled by moving the card toward and away from the camera and reimaging it on the camera. The uniform constant phase offset of the grating was controlled by the camera aperture and test card illumination.

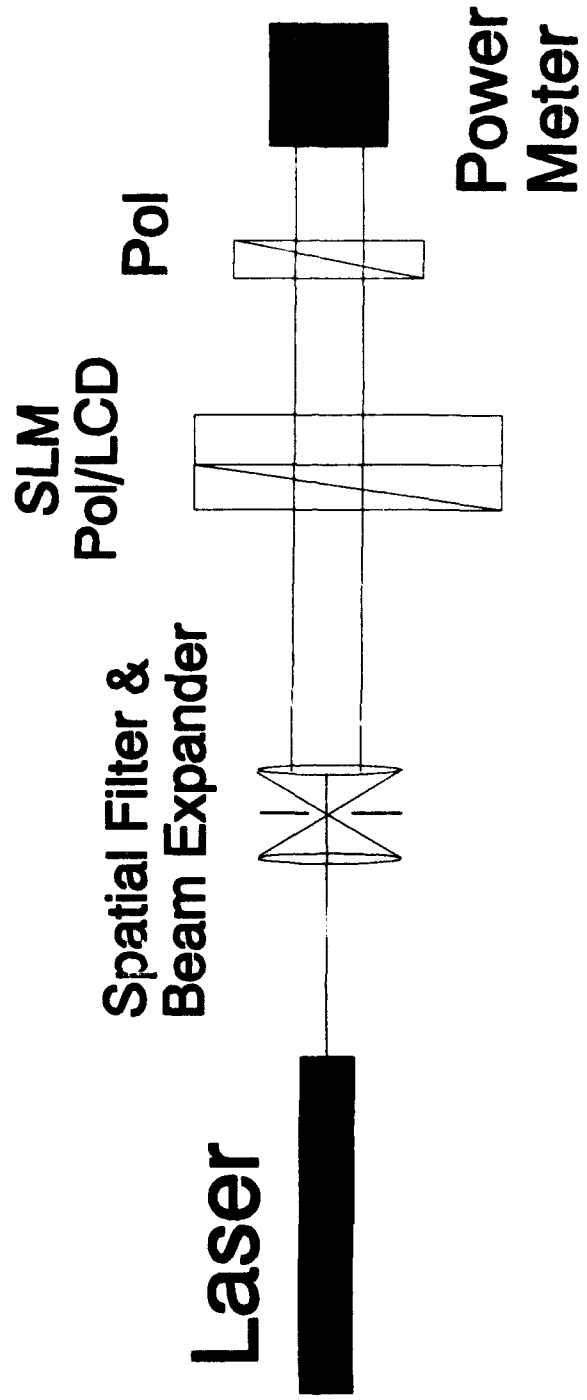

Figure 7. Apparatus to Measure Amplitude Modulation

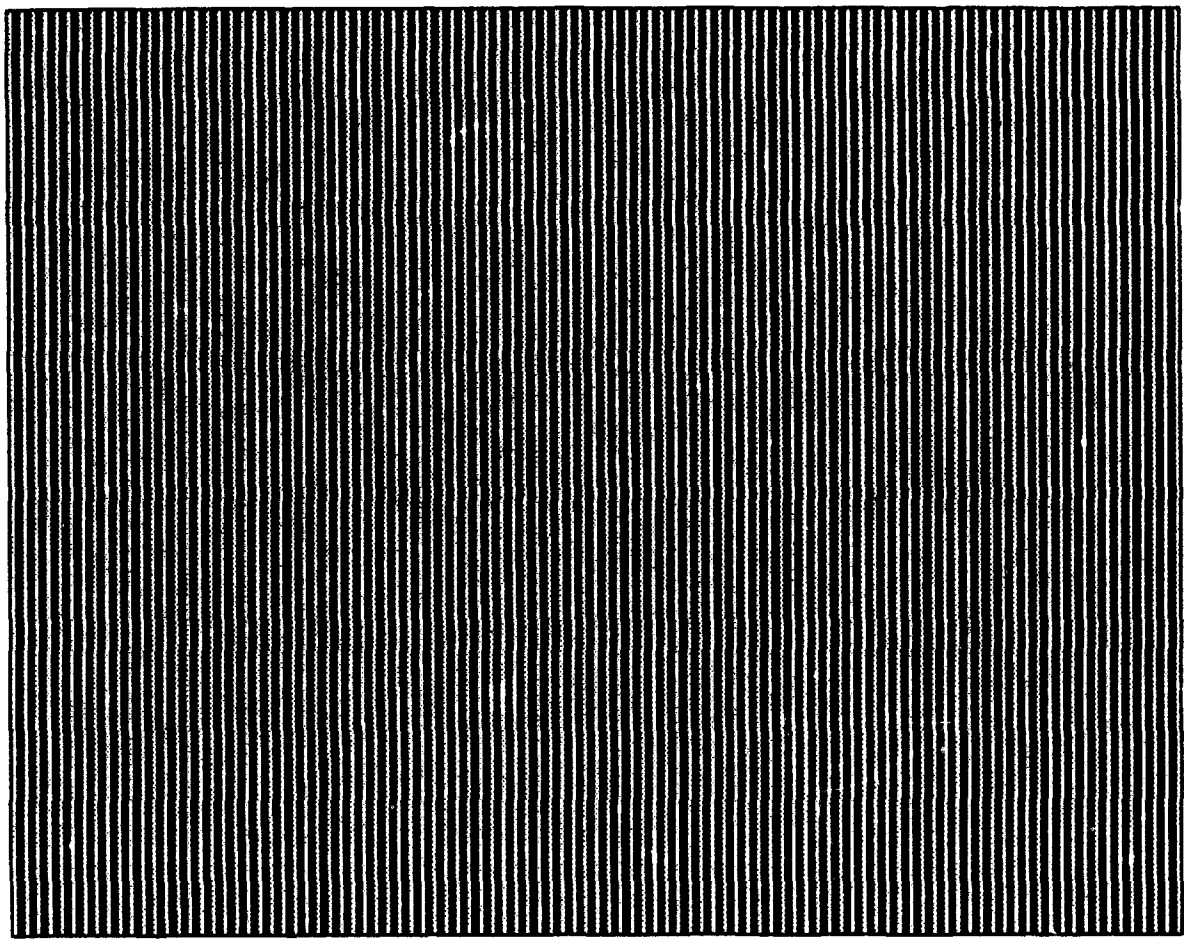

Figure 8. Striped Test Card

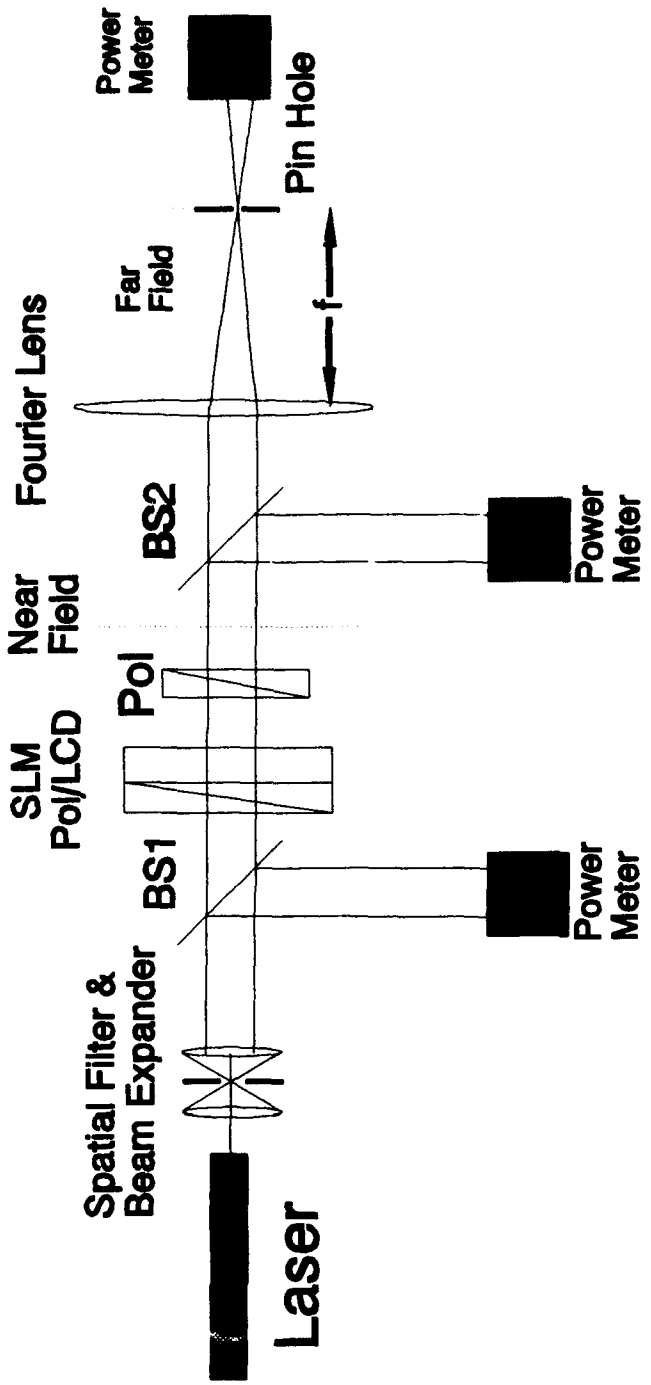

Figure 9. Apparatus to Analyze Phase Grating

The phase grating was analyzed using two techniques. First the interference fringes intensity profile data from BEAMCODE was translated to, and analyzed by, ZAPPC Fringe Analysis software, available from a Zygo interferometer (PTI). The second technique used the apparatus shown in Figure 9. The intensity profile was recorded at the two locations marked "Near Field" and "Far Field".

The Far Field intensity pattern, obtained via BEAMCODE, provided a qualitative assessment of the phase grating. To obtain a quantitative measure of the effectiveness of the phase grating, the variation of power in the central lobe (a dc component) was measured as a function of the television signal strength. This was done by placing a pinhole in the far field pattern. The power at beam splitters 1 and 2 and the power in the central lobe were measured several hundred times at each setting of the television signal strength. This isolated the phase grating effect from the fluctuations in laser output power and the transmission of the SLM.

Optimization of Phase Shifter

The nonuniform transmission properties of the SLM diffracted a large amount of power away from the central lobe and prevented the optimization of the phase shifter. The intended experiment would have used the apparatus in Figure 10. This is an adaptation of the apparatus in Figure 6.

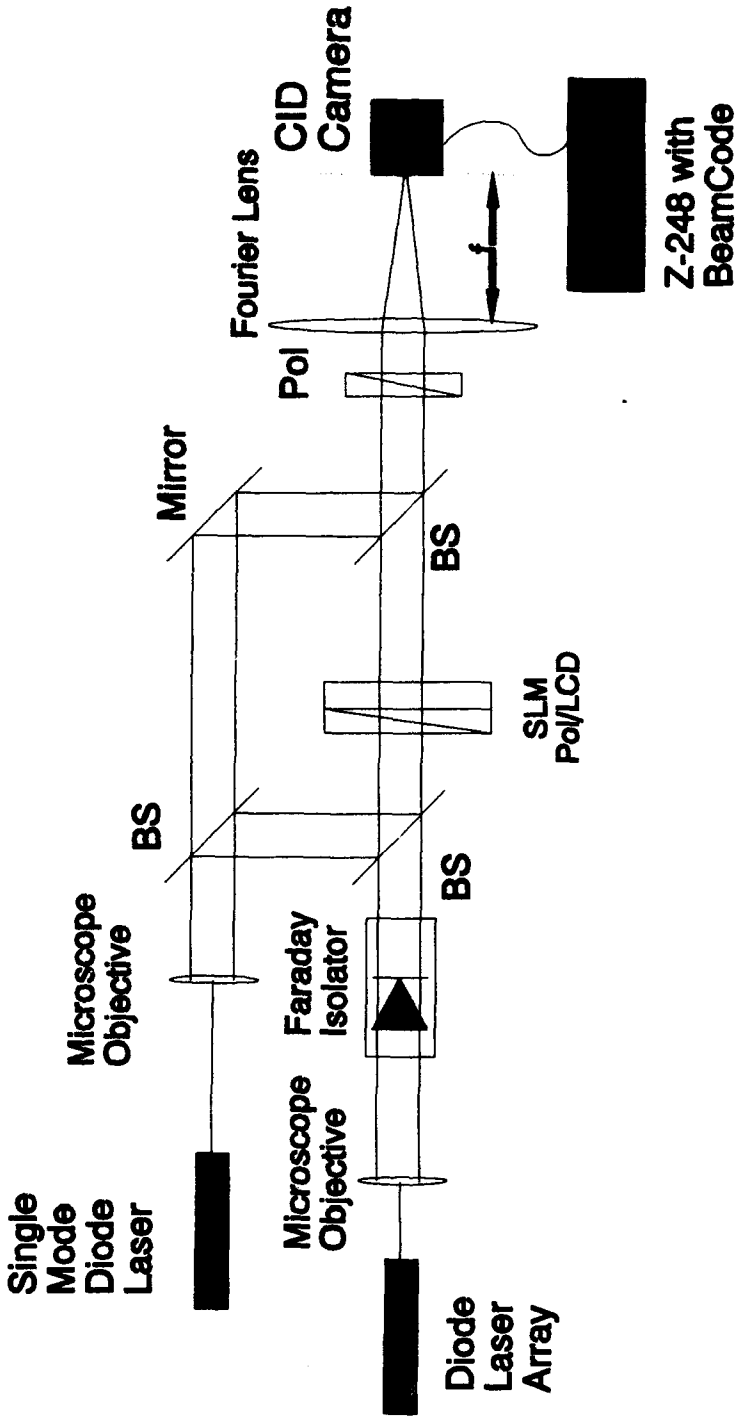

Figure 10. Apparatus to Form Single Lobe in Far Field

The microscope objective, following the diode array, was to image the array near field onto the SLM. The Fourier lens would have formed the far field intensity pattern onto the "Beam Code" camera. The single mode Sharp diode laser (LT015MFO, λ = 830 nm) would have been used to analyze the phase grating. The single-mode laser has the same wavelengths as the array, but it has a much longer coherence length and was much more suitable for interferometry. Several of the previously mentioned variables would have been optimized to produce the greatest amount of power in the central lobe.

IV. EXPERIMENTAL RESULTS

Characterization of the SLM became the primary emphasis of this thesis. Nonuniformities in the SLM as well as its very limited phase shifting capability prevented the completion of the original objective. It may still be possible to phase shift the near field radiation pattern of a diode laser array using a better SLM.

The SLM made from the Realistic television was characterized extensively. In addition to the Realistic televis[illegible], preliminary investigations were also performed on the Sony television. It was found to have even worse optical properties and was not characterized further. Unless specifically stated otherwise, all of the results in this report are from the Realistic television.

Nonuniformity

The nonuniform transmission (λ=632 nm) of the SLM can be seen in the SLM near field intensity pattern shown in Figure 11. The horizontal pattern disappeared as the "brightness" was decreased. The stronger vertical pattern remained for all settings of "brightness". Assuming that the amplitude modulation can be modeled as an infinite series of two-dimensional Rect functions.

$$E_{near}(x,y) = E_{near}(0,0) \cdot \sum_{n=-\infty}^{\infty} rect\left(\frac{x-an}{b}\right) \cdot \sum_{m=-\infty}^{\infty} rect\left(\frac{y-cm}{d}\right), \qquad (4)$$

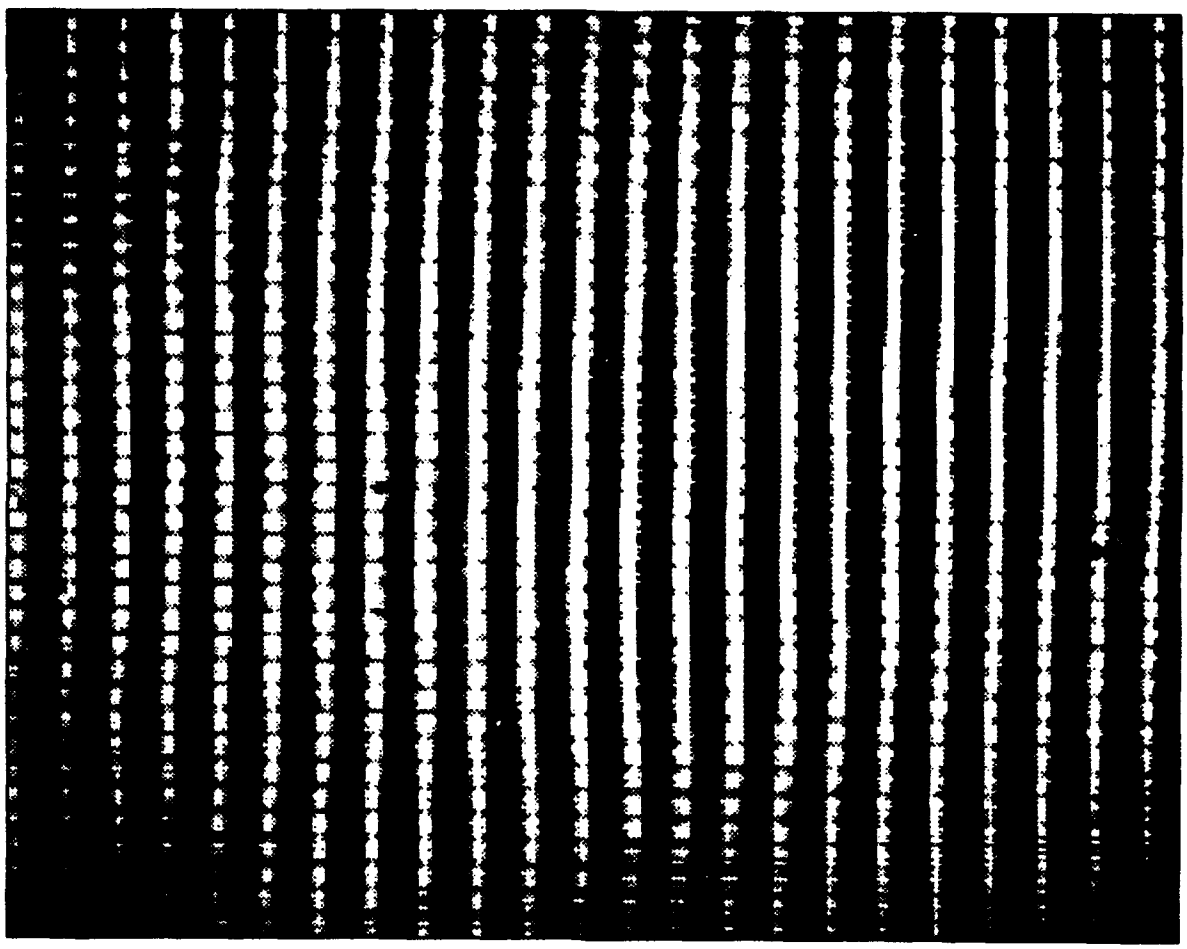

Figure 11. SLM Near Field Intensity Pattern

where

$$rect\left(\frac{x-x_o}{b}\right) = \begin{cases} 0, & \left|\frac{x-x_o}{b}\right| > \frac{1}{2} \\ \frac{1}{2}, & \left|\frac{x-x_o}{b}\right| = \frac{1}{2} \\ 1, & \left|\frac{x-x_o}{b}\right| < \frac{1}{2} \end{cases}, \tag{5}$$

For a sketch of rect(x) see Figure 12.

with
- x, y = Position coordinates along the horizontal and vertical axis in the plane of the modulator,
- b, d = Width, height of the high transmission bars, and
- a, c = Distance between bars.

Then the far field intensity pattern, which is given by a Fourier transform (calculated in Appendix C) of the near field or the transmission function turns out to be

$$I(f_x, f_y) = I_o \cdot sinc(bf_x) \cdot comb(af_x) \cdot sinc(df_y) \cdot comb(cf_y), \tag{6}$$

where

$$f_x = \frac{x_f}{\lambda f}, \quad f_y = \frac{y_f}{\lambda f}, \tag{7}$$

$$sinc\left(\frac{x-x_o}{b}\right) = \frac{\sin \pi\left(\frac{x-x_o}{b}\right)}{\pi\left(\frac{x-x_o}{b}\right)}, \tag{8}$$

For a sketch of sinc(x) see Figure 12.

with
- I_0 = Intensity at $f_x = f_y = 0$,
- x_f, y_f = Position coordinates along the horizontal and vertical axes in the focal plane,
- λ = Wavelength, and
- f = Focal length.

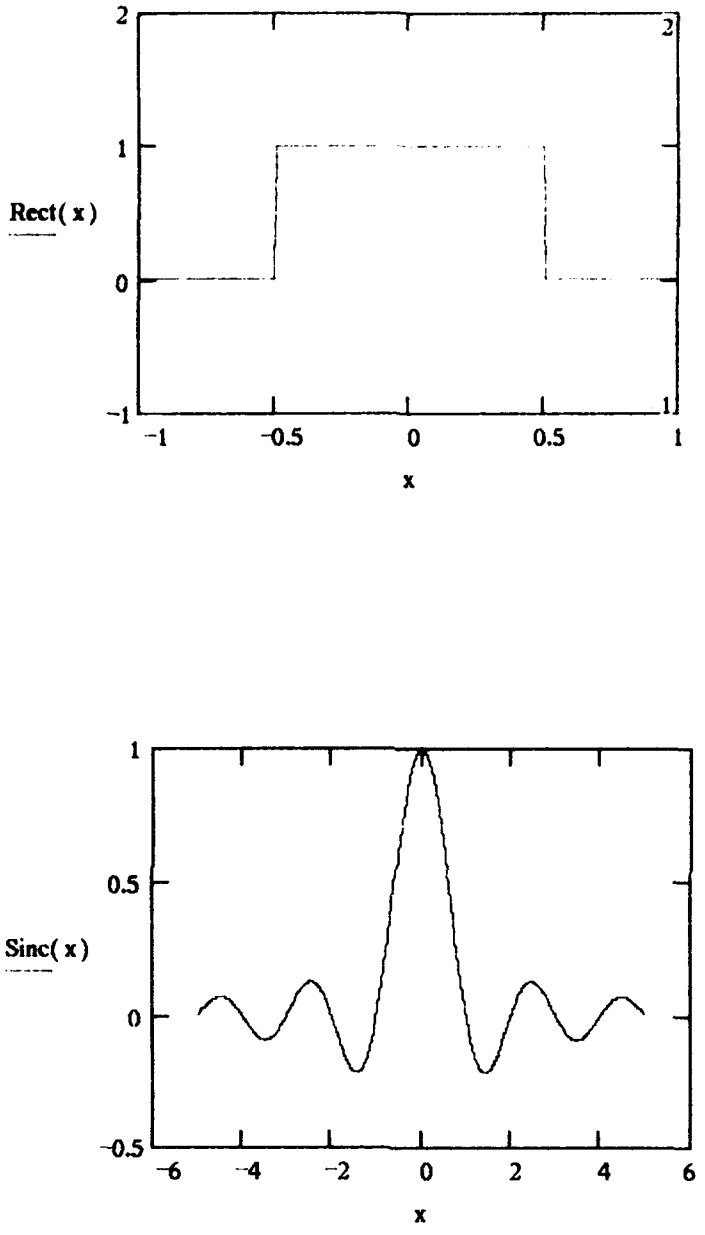

Figure 12. Rect (Top) and Sinc (Bottom) Functions

This corresponded well to the observed far field intensity pattern as shown in Figure 13. The far field pattern contained a two-dimensional comb function within a slowly varying envelope that was similar to the sinc squared function.

The effect of this nonuniformity also appeared in a typical fringe pattern, recorded using the Mach-Zehnder Interferometer, as shown in Figure 14. The large horizontal fringes are caused by a slight tilt in the interferometer. The vertical fringe pattern and the bending of the fringes are caused by the nonuniformity of the SLM. The vertical bars move when the SLM is translated across the beam. Translation of the SLM also shows that the fringe pattern bends more than the fringe separation distance. This means that the SLM had a slowly varying phase nonuniformity greater than one wave. This might cause a problem in experiments that use a large portion of the SLM. For the characterization work, with a one centimeter beam, the phase nonuniformity had little adverse effect compared to the strong effect of the amplitude grating. The irregularities in the interference pattern, caused by the amplitude transmission nonuniformities of the SLM, prevented the ZAPPC software from analyzing any phase grating.

Phase Shift

The SLM was able to produce minimal phase shifting. The interference fringe pattern from the Mach-Zehnder interferometer

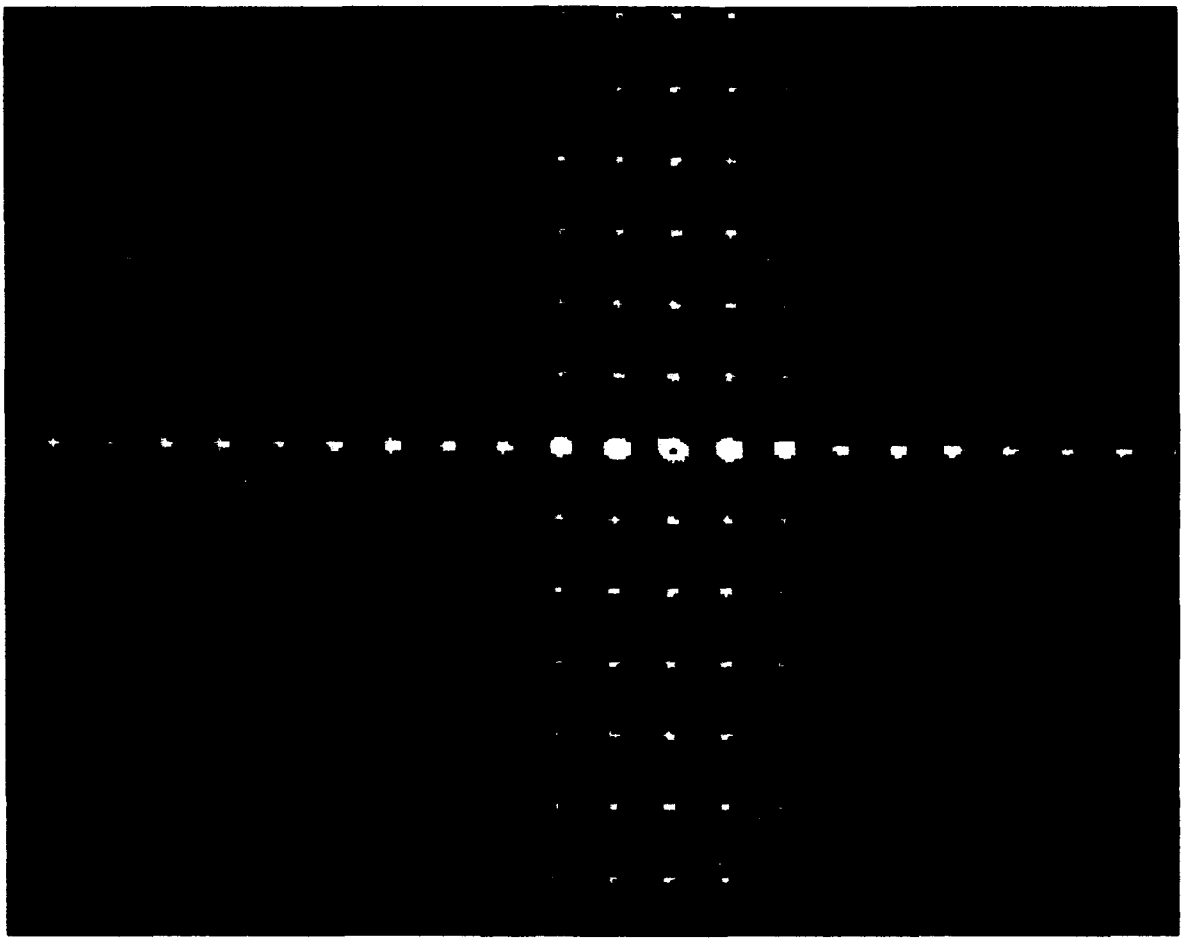

Figure 13. SLM Far Field Intensity Pattern with Uniform Video Signal

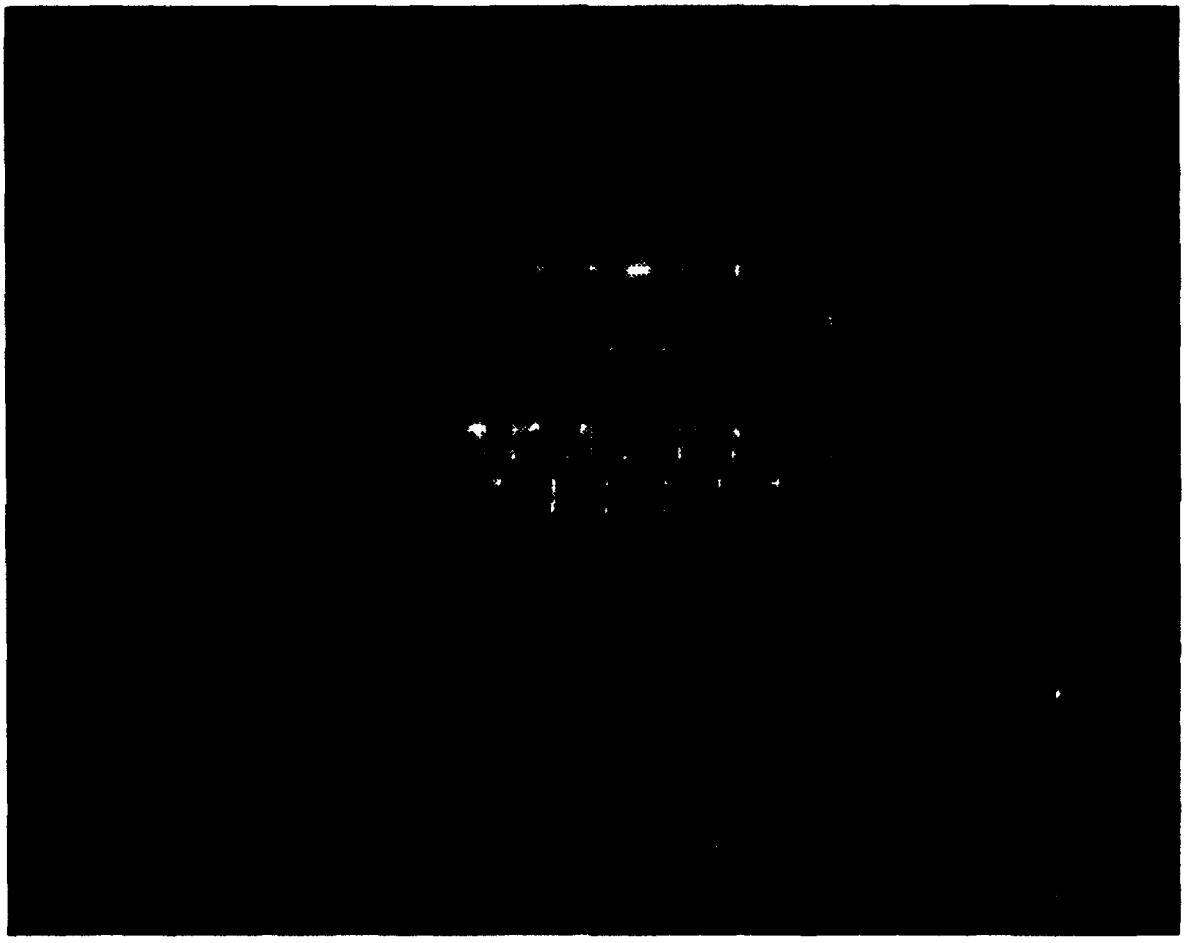

Figure 14. Interference Fringes from Mach-Zehnder Interferometer

would move with either a change in the brightness control voltage or the uniform signal voltage.

Figure 15 shows a family of curves for phase shift vs. brightness at several different wavelengths. The amount of phase shift was obtained by capturing a series of images as the brightness was varied. This image data was transferred to a Sun workstation where MATLAB software was used to produce grey scale intensity printouts as can be seen in Figure 16. MATLAB was also used to perform some simple digital image processing. Figure 16 shows how, at a wavelength of 488 nm, strong diffraction almost completely obscures the fringe pattern. The fringe pattern was enhanced by finding the average intensity, of all the images, at each point. This average image was then subtracted from individual images to produce improved fringe patterns as shown in Figure 17.

A series of these printouts was then used to track the shift of the fringe pattern. Tracking the movement of all three fringes shown in Figure 17 provided the mean and standard deviation of the phase shift shown in Figure 15. The large error bars represent the uncertainty in assigning an arbitrary position to a fringe in a poor quality image.

Visual inspection of the fringe pattern, displayed on a television screen, showed that the fringes drifted with time. Rapidly capturing the fringe images on computer tended to reduce, but not eliminate, this drift. The data shown in Figure 15 are for single trials and the error bars do not include the

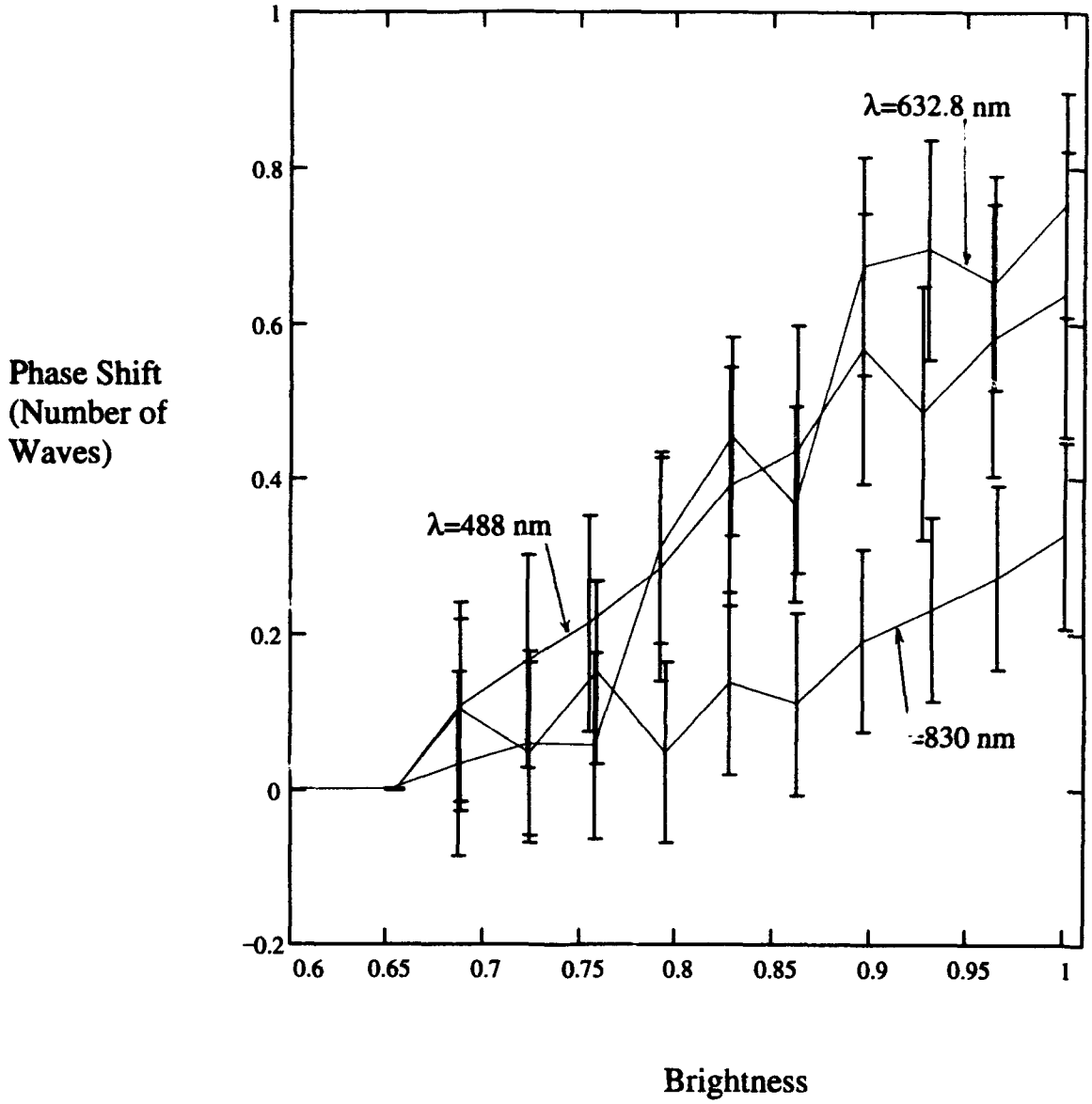

Figure 15. Phase Shift vs Brightness

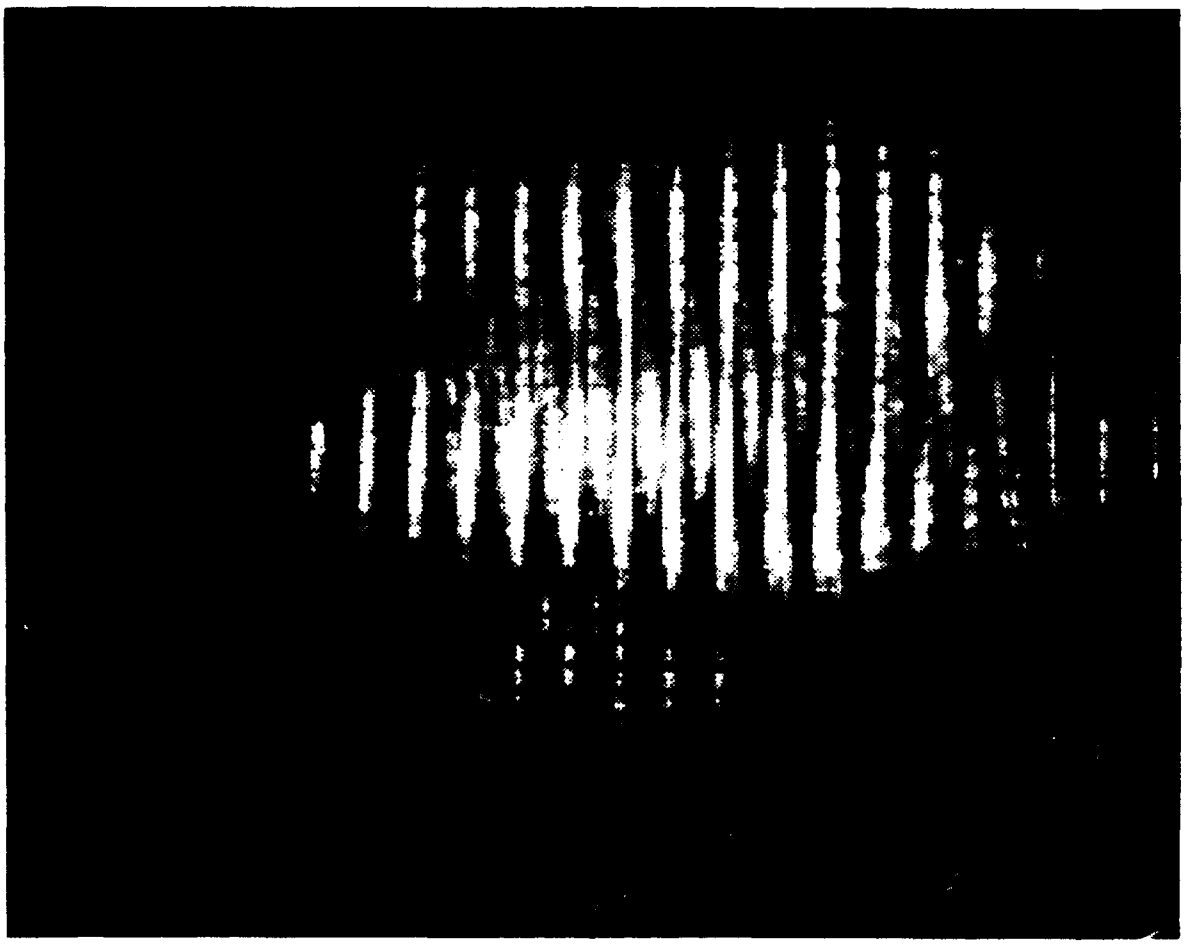

Figure 16. Grey Scale Raw Fringe Pattern

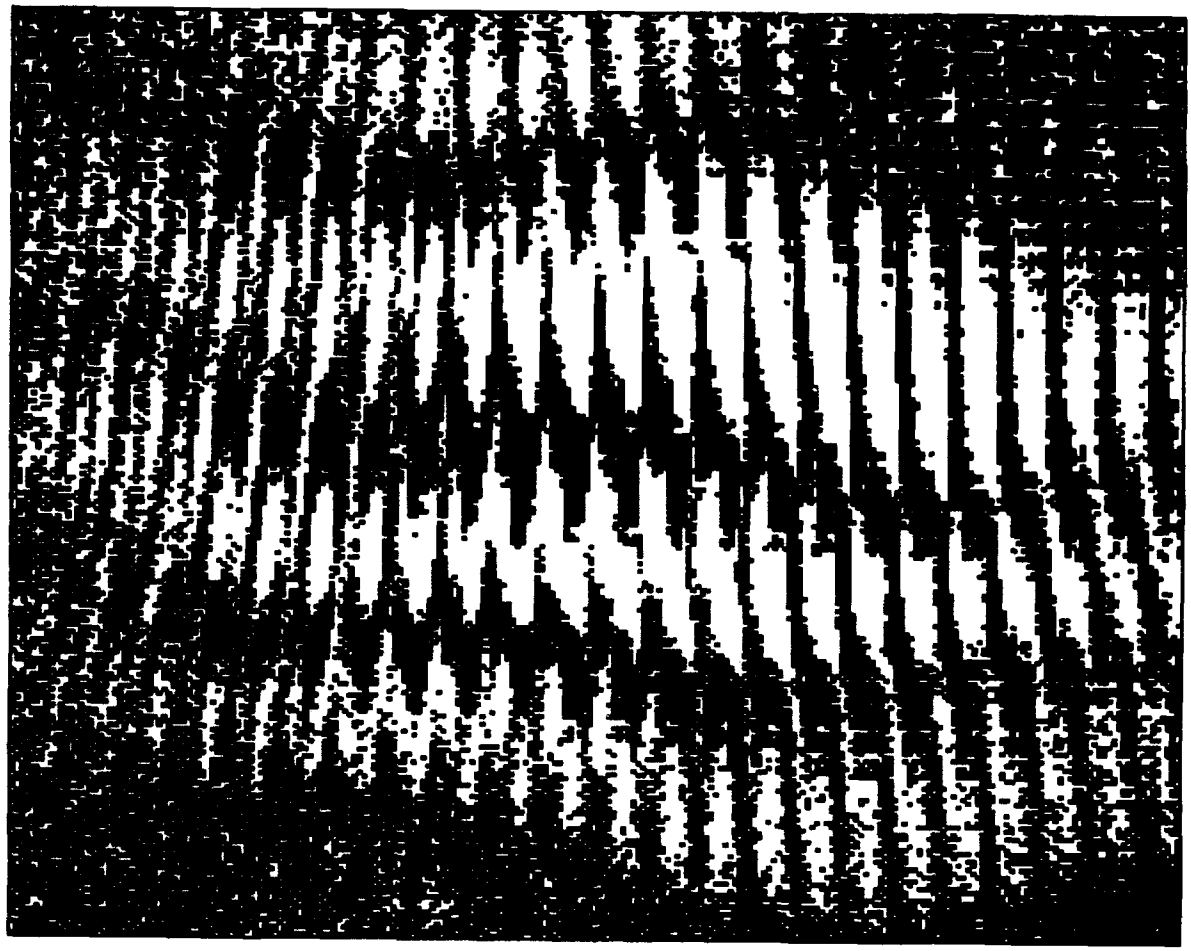

Figure 17. Enhanced Fringe Pattern

uncertainty in the fringe position from one trial to the next. Visual inspection of the fringes, with changing brightness settings, confirmed the general shape of the phase shift curve. The shift starts at an approximate brightness of 0.65 and peaked at a brightness of one. The exact amount of phase shift is highly questionable.

Initial characterization of the Sony/Sharp SLM produced the faint fringe pattern shown in Figure 18. The enhanced fringe pattern is shown in Figure 19. The Sony SLM was only able to produce approximately 50% of a wave of phase shift, at λ=488 nm, compared to 60% for the Realistic SLM. This limitation, along with the even stronger pixel diffraction problem, eliminated the Sony SLM as a contender for a phase shifter.

Quantifying the amount of phase shift vs change in brightness was the initial step in characterizing the SLM. However, it was the phase shift associated with a change in the television signal voltage (much smaller dynamic range than brightness control voltage) that was critical to the formation of an SLM. Varying the amount of light to the Cohu camera, and hence the uniform television video signal, produced only 4% to 7% of wave phase shift, at λ=632.8 nm.

The second technique, measurement of power in the central lobe to quantify the phase modulation index, required the creation of a phase grating. The grating was made by varying the index of refraction from one pixel to the next using the television signal voltage. The brightness control voltage was

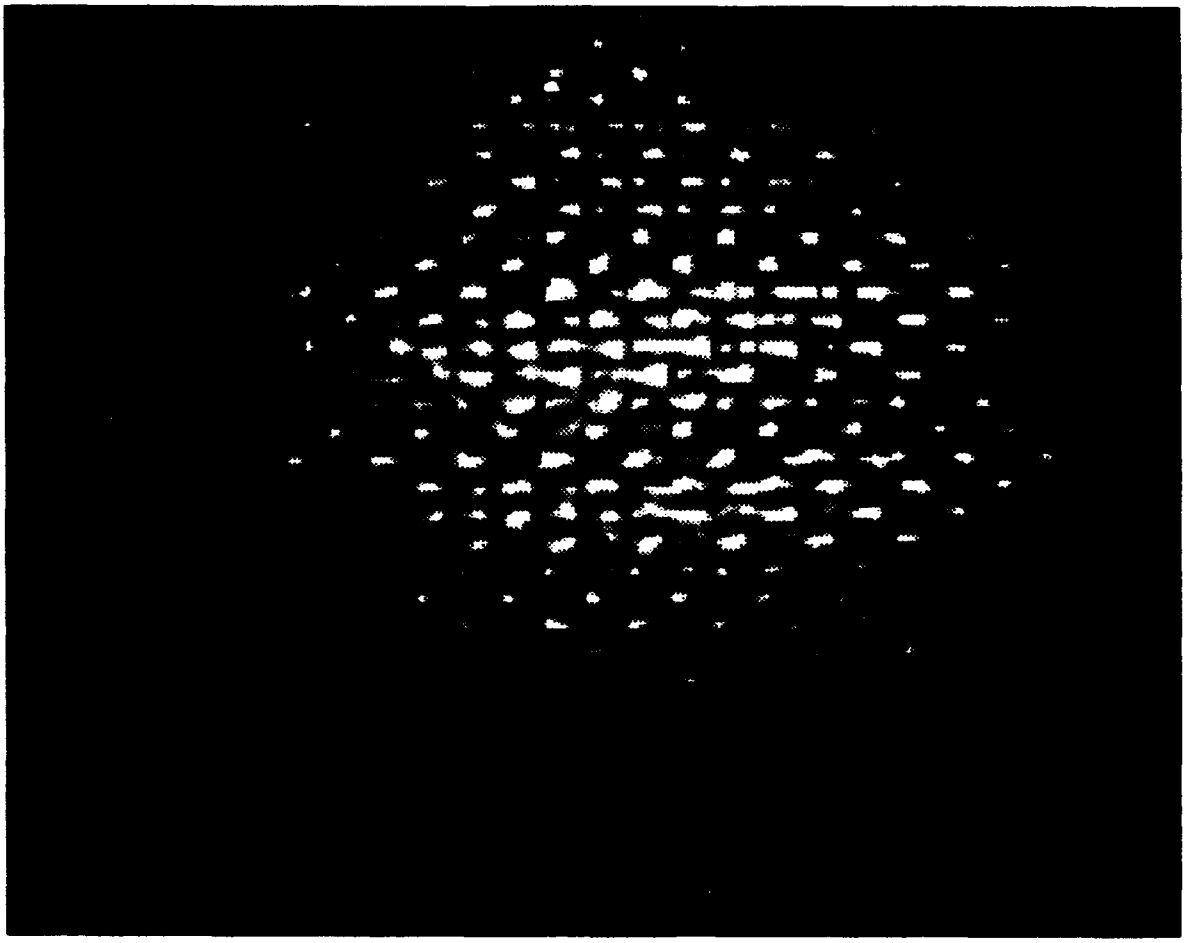

Figure 18. Fringe Pattern Using Sony SLM (λ=488 nm)

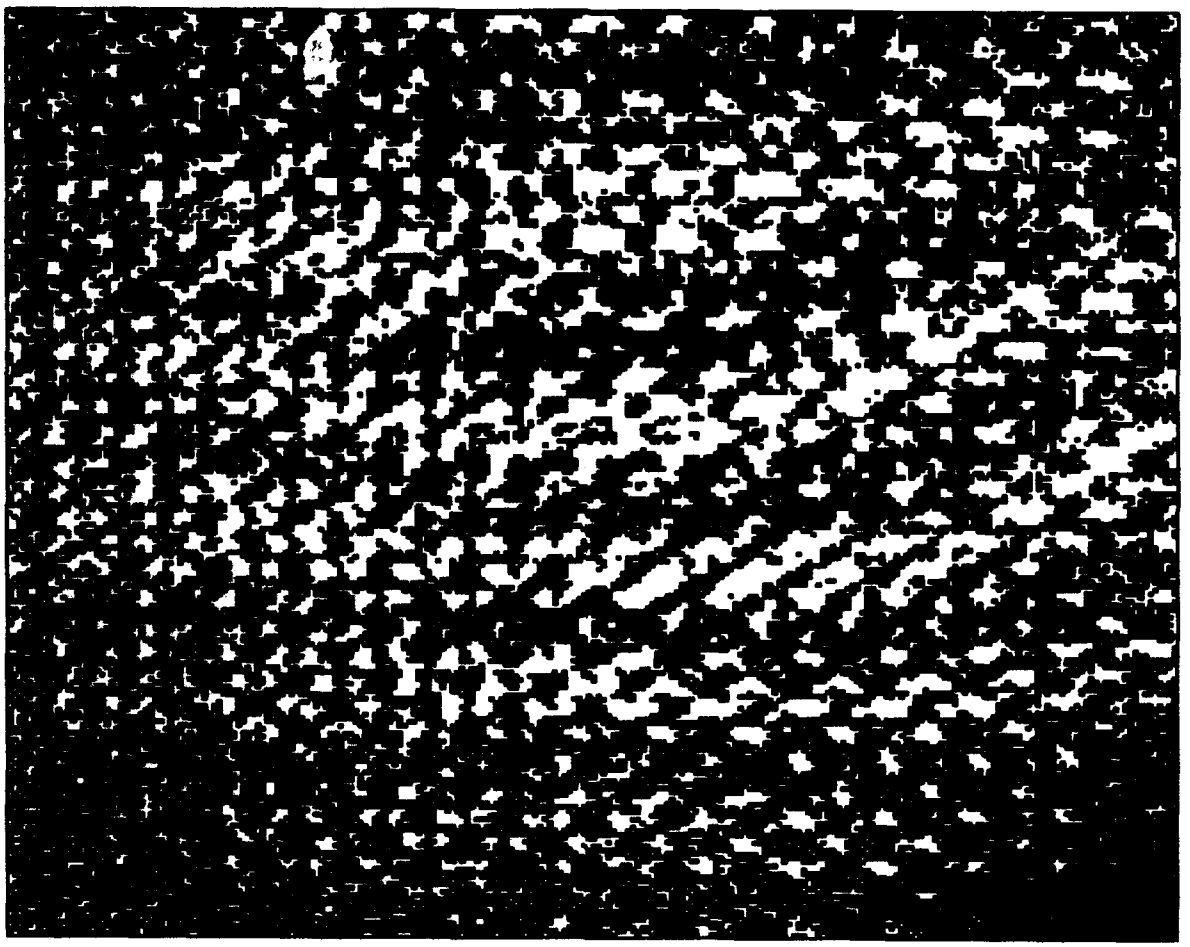

Figure 19. Enhanced Fringe Pattern Using Sony SLM

common to all pixels and had no apparent direct impact on the effectiveness of the grating. So the phase shift measured with the second technique should only be compared to the 4 to 7% phase shift, associated with a change in signal voltage, found using the Mach-Zehnder interferometer.

Observation of an oscilloscope trace of the television signal confirmed that the striped test card was able to produce a sinusoidally varying signal as can be seen in Figure 20. If the corresponding sinusoidally varying phase grating were the only feature of the transmittance function of the SLM, we would expect the far field radiation pattern to be[11]

$$\frac{E(f_x,m)}{E_o} = \sum_{q=-\infty}^{\infty} J_q\left(\frac{m}{2}\right) \delta(f_x - qf_o) \ , \qquad (9)$$

where m = Peak to peak phase shift of the grating,
f_0 = Frequency of the grating, and
E_0 = Intensity at $f_x = 0$, $m = 0$.

The far field intensity pattern would be

$$\frac{I(f_x,m)}{I_o} = \left[\sum_{q=-\infty}^{\infty} J_q\left(\frac{m}{2}\right) \delta(f_x - qf_o)\right]^2 \ , \qquad (10)$$

where I_0 = Intensity at $f_x = 0$, and $m = 0$.

However, when the sinusoidally varying phase grating is multiplied by the previously mentioned amplitude grating the combined effect in the far field intensity pattern is much more complicated (see Appendix D for details).

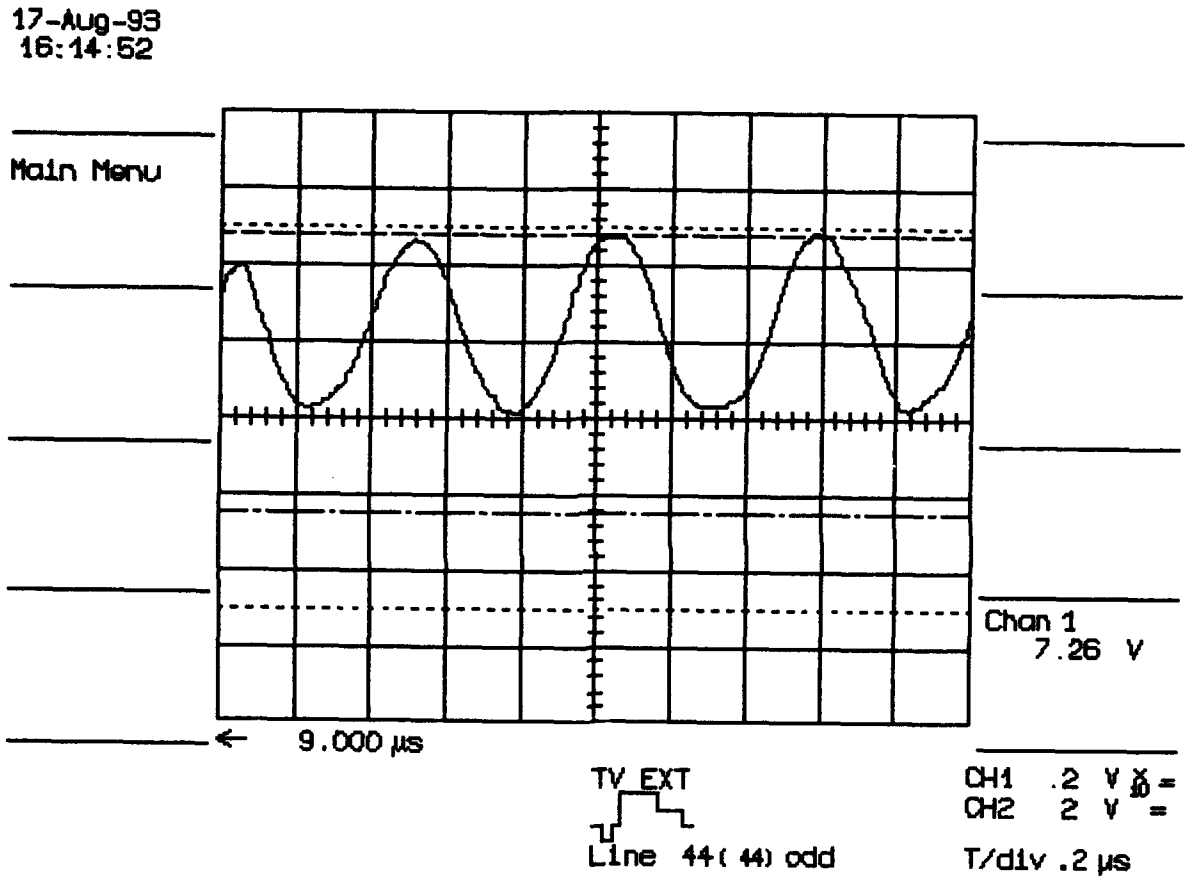

Figure 20. Sinusoidally Varying Television Video Signal

$$\frac{I(f_x,m)}{I_o} = \left[\sum_{q=-\infty}^{\infty} J_q\left(\frac{m}{2}\right) sinc[b(f_x-qf_0)] \cdot comb\ [a(f_x-qf_0)]\right]^2 \quad (11)$$

This may be interpreted as a summation of comb functions similar to the far field pattern without a phase grating. Each comb function is weighted by a corresponding Bessel function and offset by an integer multiple of f_0. The frequency of the phase grating was approximately half the frequency of the amplitude grating. This would cause new high intensity points, corresponding to the odd terms, to appear halfway between the previous points, along the horizontal axis, as is evident in Figure 21.

The central lobe where $f_x = 0$, is composed of several terms.

$$\frac{I(0,m)}{I(0,0)} = \left[J_0\left(\frac{m}{2}\right) + 2J_2\left(\frac{m}{2}\right) sinc(b2f_o) + 2J_4\left(\frac{m}{2}\right) sinc(b4f_o) + \ldots\right]^2 \quad (12)$$

For small values of its argument, the zeroth order Bessel function is much larger than any of the higher order Bessel functions. So the intensity in the central lobe, as a function of the degree of phase shift in the phase grating, may be simplified to

$$\frac{I}{I_o} = J_o^2\left(\frac{m}{2}\right), \quad (13)$$

where I_0 is the intensity in the central lobe in the absence of any phase modulation, i.e. m=0.

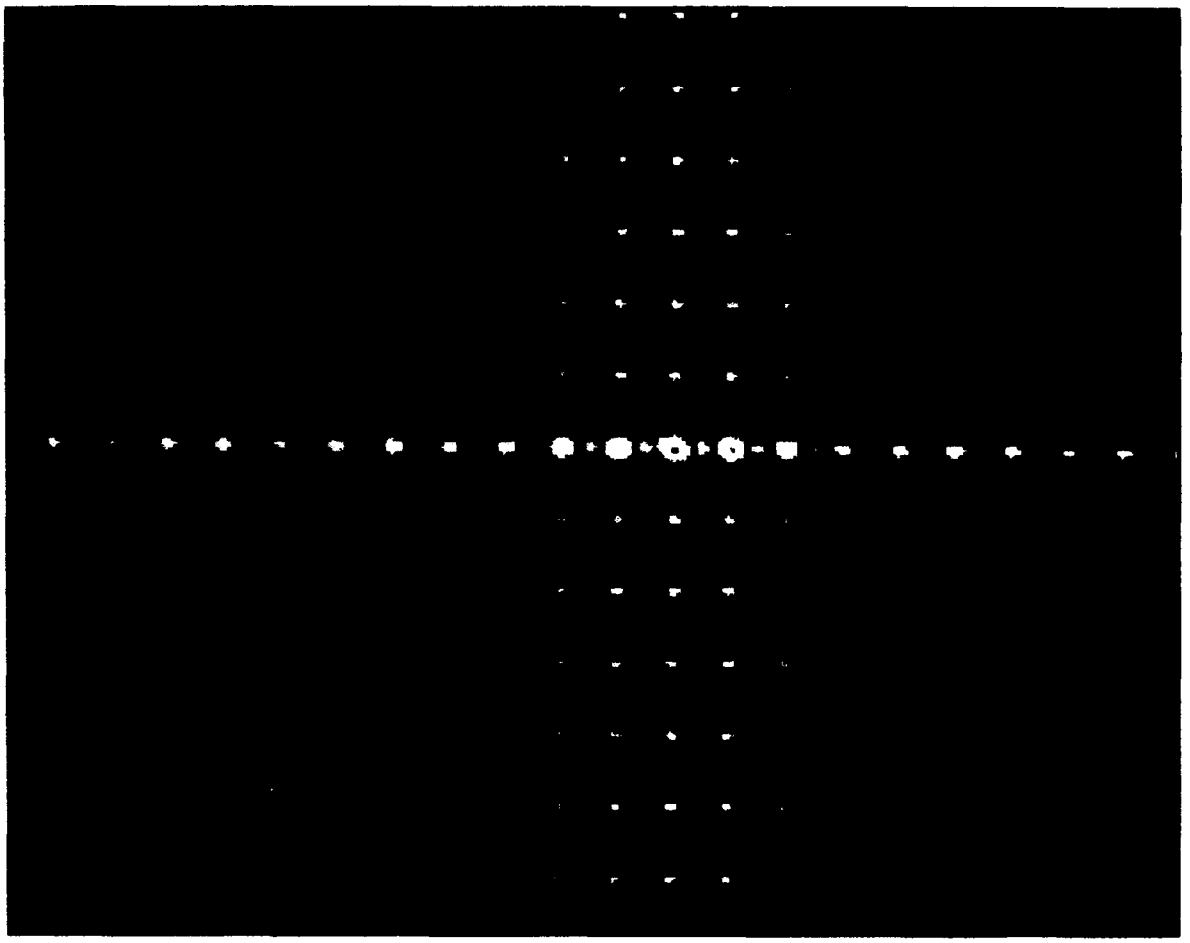

Figure 21. SLM Far Field Pattern With Phase Grating

Figure 22 shows the amount of change of power in the central lobe as a function of the signal voltage (λ=632 nm). This shows that the intensity drops by approximately 3% from minimum signal to maximum signal. This corresponds to an m of 0.48 radians or 7.6% of a wave and agrees with the previous calculation of maximum phase shift using the signal voltage.

Polarization Rotation

The polarization rotation characteristics of the Realistic SLM, obeying Malus' Law, can be seen in Figure 23.

$$I(\theta) = I(\theta_o)\cos^2(\theta - \theta_o) \ , \qquad (14)$$

where θ *is the orientation angle of the polarizer, and* θ_0 is an arbitrary reference angle.

The solid line is the result of two polarizers followed by the liquid crystal cell (LCC). The dashed line is the result of the liquid crystal cell between two polarizers. The first polarizer forms linearly polarized light. The LCC rotates the polarization 90^0, thus the analyzing polarizer experiences the same effect as if the original polarizer, without SLM, were rotated by 90^0. This is evident in the 90^0 offset between the two curves in Figure 23.

Amplitude Modulation

The SLM worked well as an amplitude modulator, which was no surprise since this is the application for which it was designed.

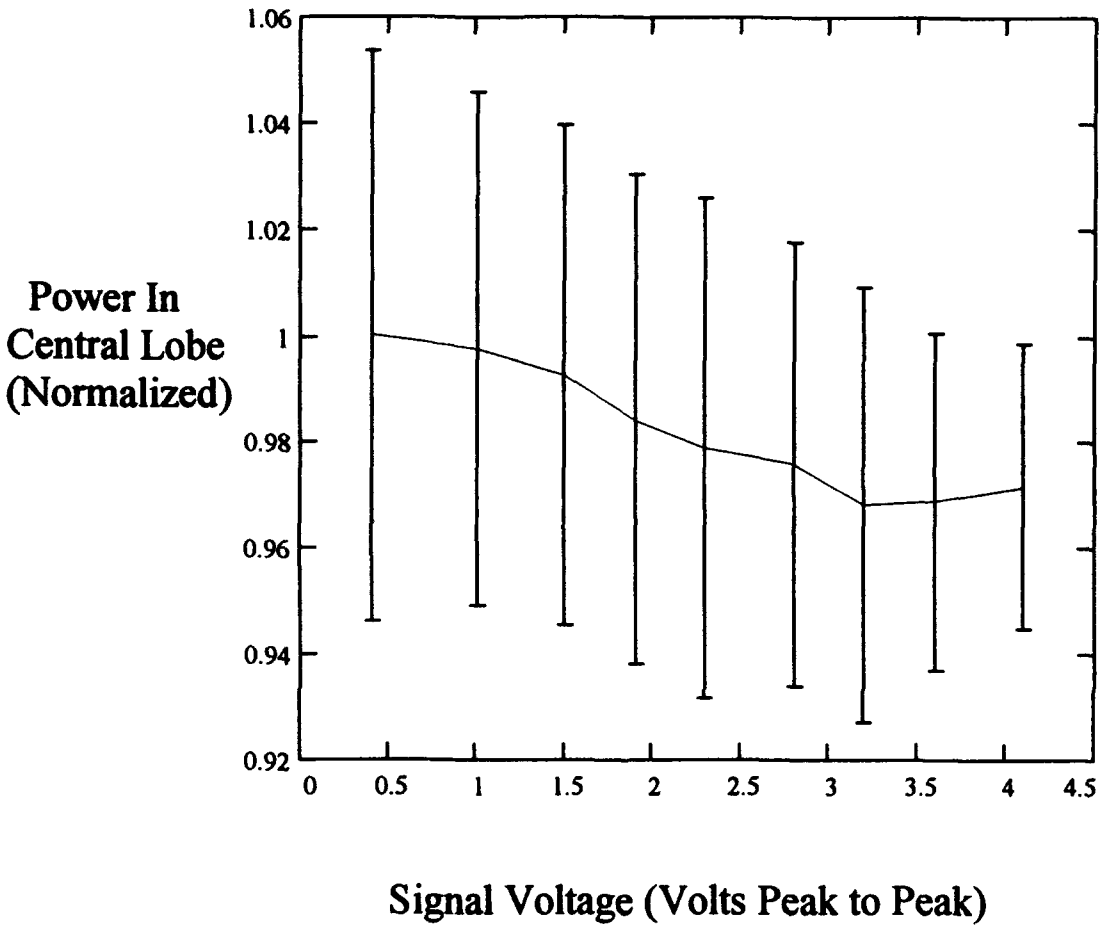

Figure 22. Power in Central Lobe vs Signal Voltage

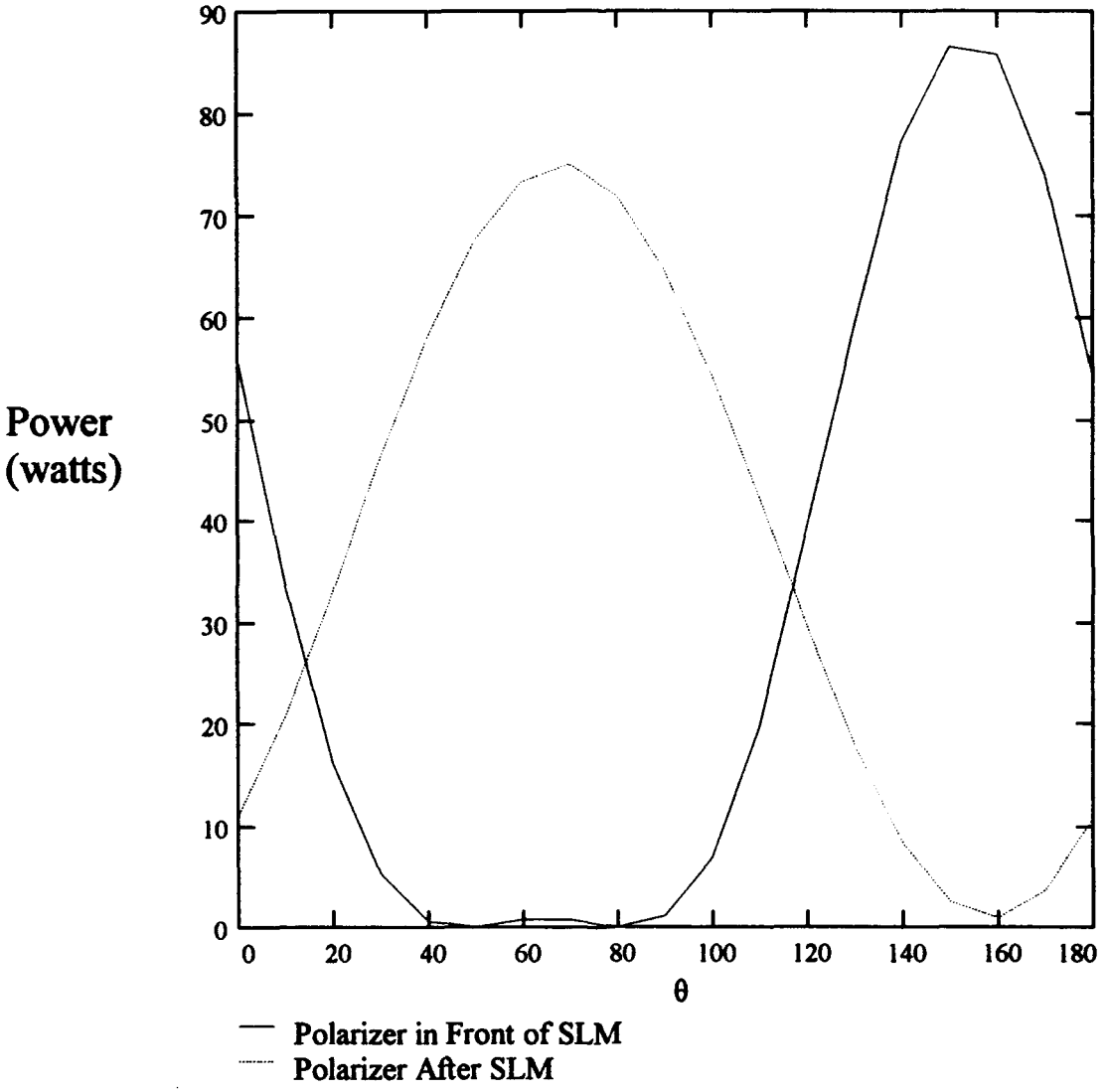

Figure 23. Power vs Orientation of Polarizer

Figure 24 shows the rapid increase in transmission above a certain threshold of brightness (applied voltage). The amplitude modulation results correspond nicely, with a little less structure, to previous research (Figure 5).

Array Near Field

The array near field was imaged onto the BEAMCODE camera. The light from the laser diode array is highly astigmatic limiting the ability of a single spherical lens to image the array near field. The image shown in Figure 25 is a compromise between the horizontal and vertical focus settings. The focus is very sensitive to the object distance and insensitive to the image distance. Thus the exact position of the SLM should not have been extremely critical.

The very low amount of phase shift would not have been enough to form a single spot in the far field. However, even a 5% wave shift would have helped to move more power to the center of the double lobe pattern. The very strong amplitude diffraction grating would have completely destroyed any small improvement that a slight phase grating would have created.

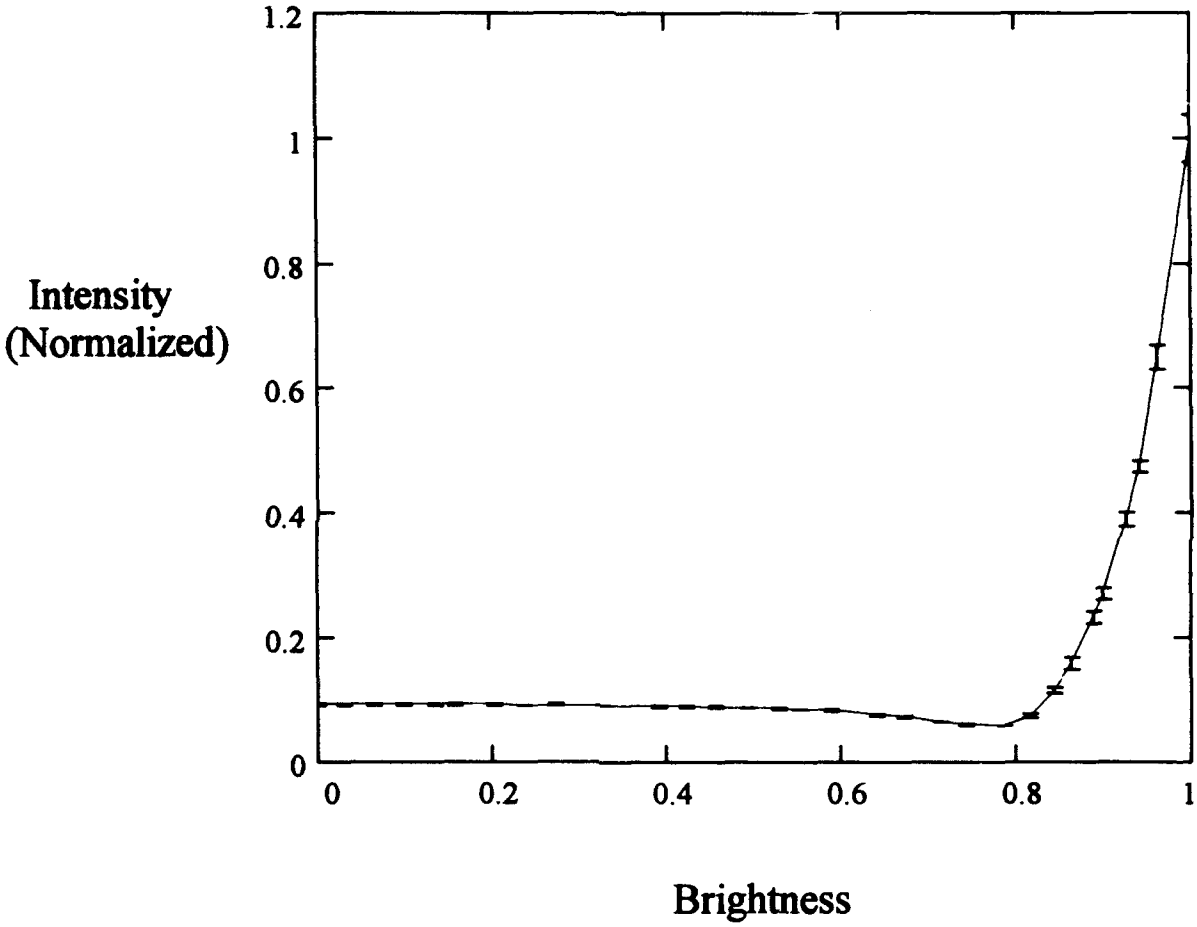

Figure 24. Amplitude Modulation with Parallel Polarizers (λ=632.8 nm)

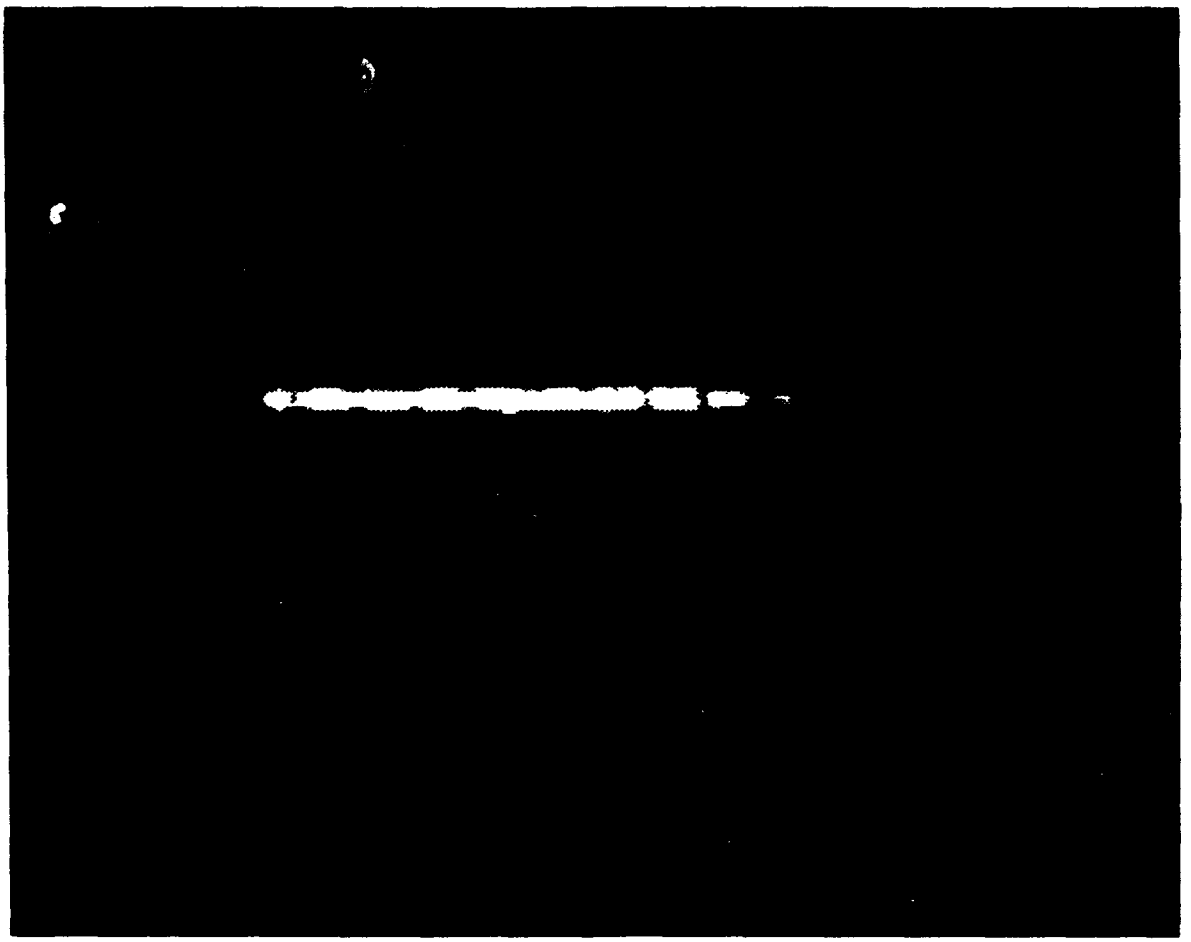

Figure 25. Array Near Field Intensity Pattern

V. CONCLUSIONS/RECOMMENDATIONS

Inexpensive liquid crystal displays with a strong pixel to pixel amplitude modulation are not suitable to be used as Spatial Light Modulators for the purpose of altering the phase front of a laser beam. Optical flats attached to the SLM, back filled with an index matching material, should eliminate some of the slowly varying phase nonuniformities. However, the amplitude grating will still destroy any image being passed through the SLM.

Altering the phase front of a diode laser array to produce a single spot in the far field is still a valid experiment that should be investigated. A very high quality SLM is required and attempts to modify inexpensive LCD displays found in commercial pocket televisions should be avoided.

REFERENCES

1. D.E. Ackley, D. Botez, and B. Bogner, "Phase-Locked Injection Laser Arrays with Integrated Phase Shifters," RCA Rev. 44, 625 (1983)

2. C.P. Cherng and M. Osiński, "Fundamental Array Mode Operation of Semiconductor Laser Arrays Using External Spatial Filtering," in Laser Diode Technology and Applications III, (SPIE). 1418, 372-385 (1991)

3. S. MacCormack and J.W. Eason, "Near-Diffraction-Limited Single Lobe Emission From a High-Power Diode-Laser Array Coupled to a Photorefractive Self-Pumped Phase-Conjugate Mirror," Optics Letters. 16, 705-707 (1991)

4. S. Thaniyavarn and W. Dougherty, "Generation of a Single-Lobed Radiation Pattern From a Phased-Array Laser Using a Near-Contact Variable Phase-Shift Zone Plate," Electronics Letters. 23, (1987)

5. M. Matsumoto, M. Taneya, S. Matsui, S. Yano and T. Hijikata, "Single-Lobed Far-Field Pattern Operation in a Phased Array with an Integrated Phase Shifter," Appl. Phys. Lett. 50, 1541-1543, (1987)

6. S. Mukai, M. Watanabe, H. Itoh, and H. Yajima, "Integration of a Diode Laser as an Electronic Lens for Contrclling the Beam Focus Position," Appl. Phys. Lett. 54, 315-316, (1989)

7. H. Itoh, S. Mukai, F. Sauer, M. Watanabe, and H. Yajima, "Fringe Shifting of Phase-Coupled Array Lasers for Optical Logic Operations," Int Journal of Optical Computing. 2, 89-96, (1991)

8. K. Tatsuno, R. Drenten, C. van der Poel, J. Opschoor, and Gerard Acket, "Diffraction-Limited Circular Single Spot From Phased Array Lasers," Appl. Opt. 28, 4560-4568, (1989)

9. M. Williams, "Laser Power Beams Obtained by the Dynamic Selection of Emitting Elements in an Array," Appl. Opt. 31, 2738-2742, (1992)

10. J.T. Verdeyen, *Laser Electronics, Second Edition* (Prentice Hall, Englewood Cliffs, New Jersey, 1989), Chap. 13, pp. 497-503

11. J.W. Goodman, *Introduction to Fourier Optics* (McGraw-Hill, San Francisco, 1968), Chap. 4, pp. 61-70

12. B. Bahadur, "Liquid Crystal Displays," Mol. Cryst. Liq. Cryst. 109, 3-98, (1984)

13. N. Konforti, E. Marom, and S.T. Wu, "Phase-only Modulation with Twisted Nematic Liquid-Crystal Spatial Light Modulators," Optics Letters. 13, 251-253, (1988)

APPENDIX A - Calculation of Far Field from In-Phase Near Field

The electric field of the in-phase array mode, for an array with an even number of elements, may be written as (For an array mode with an odd number of elements replace the sine with a cosine)

$$E_{near}(x) = E_{near}(0) \cdot \left|\sin\left(2\pi\frac{x}{2b}\right)\right| \cdot Gaus\left(\frac{x}{c}\right), \qquad (A.1)$$

where

$$Gaus\left(\frac{x-x_o}{b}\right) = \exp\left[-\pi\left(\frac{x-x_o}{b}\right)^2\right], \qquad (A.2)$$

with
- x = Position coordinate along the horizontal axis in the near field
- 2b = Distance between elements in the array
- 2c = Approximate width of the array
- $E_{near}(0)$ = Electric field at the center of the array.

The electric field in the far field is given by the Fourier transform of the near field radiation pattern.

$$\begin{aligned} E_{far}(f_x) &= \mathcal{F}\{E_{near}(x)\} \\ &= \mathcal{F}\left\{E_{near}(0) \cdot \left|\sin\left(2\pi\frac{x}{2b}\right)\right| \cdot Gaus\left(\frac{x}{c}\right)\right\}, \end{aligned} \qquad (A.3)$$

where

$$f_x = \frac{x_f}{\lambda f}, \qquad (A.4)$$

with
- x_f = Position coordinate along the horizontal axis in the focal plane
- λ = Wavelength
- f = Focal length.

The calculation of the above Fourier transform may be simplified by first finding the Fourier transform of a single half period of the rectified cosine function. A half period of the rectified cosine function may be written as

$$t_1(x) = \cos\left(2\pi\frac{x}{2b}\right) \cdot rect\left(\frac{x}{b}\right), \qquad (A.5)$$

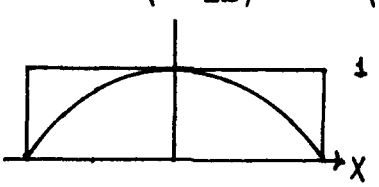

where

$$rect\left(\frac{x-x_o}{b}\right) = \begin{cases} 0, & \left|\frac{x-x_o}{b}\right| > \frac{1}{2} \\ \frac{1}{2}, & \left|\frac{x-x_o}{b}\right| = \frac{1}{2} \\ 1, & \left|\frac{x-x_o}{b}\right| < \frac{1}{2} \end{cases} . \qquad (A.6)$$

For a sketch of rect(x) see Figure 12.

The Fourier transform of a half period of the rectified cosine function may be simplified by using the identity

$$\mathcal{F}\{g(x) \cdot h(x)\} = \mathcal{F}\{g(x)\} * \mathcal{F}\{h(x)\} , \qquad (A.7)$$

and by using the Fourier transforms of the cosine and rect functions

$$\mathcal{F}\left\{\cos\left(2\pi\frac{x}{2b}\right)\right\} = \frac{1}{2}\left[\delta\left(f_x - \frac{1}{2b}\right) + \delta\left(f_x + \frac{1}{2b}\right)\right] , \qquad (A.8)$$

$$\mathcal{F}\left\{rect\frac{x}{b}\right\} = |b|\ sinc\,(bf_x) , \qquad (A.9)$$

where

$$sinc\left(\frac{x-x_o}{b}\right) = \frac{\sin\pi\left(\frac{x-x_o}{b}\right)}{\pi\left(\frac{x-x_o}{b}\right)} . \qquad (A.10)$$

For a sketch of sinc(x) see Figure 12.

The Fourier transform of a half period of the rectified cosine function simplifies to

$$\begin{aligned} \mathcal{F}\{t_1(x)\} &= \mathcal{F}\left\{\cos\left(2\pi\frac{x}{2b}\right)\right\} * \mathcal{F}\left\{rect\frac{x}{b}\right\} \\ &= \frac{1}{2}\left[\delta\left(f_x - \frac{1}{2b}\right) + \delta\left(f_x + \frac{1}{2b}\right)\right] * |b|\ sinc(bf_x) \qquad (A.11) \\ &= \frac{|b|}{2}\left[sinc\left(bf_x - \frac{1}{2}\right) + sinc\left(bf_x + \frac{1}{2}\right)\right] . \end{aligned}$$

The complete rectified cosine function may be written as a sum of offset half periods.

$$t_2(x) = \left[\begin{array}{l} \cos\left(2\pi\frac{x}{2b}\right) \cdot rect\left(\frac{x}{b}\right) \\ + \cos\left(2\pi\frac{x+b}{2b}\right) \cdot rect\left(\frac{x+b}{b}\right) + \ldots \end{array} \right] \qquad \text{(A.12)}$$

This simplifies to

$$\begin{aligned} t_2(x) &= \sum_{n=-\infty}^{\infty} \cos\left(2\pi\frac{x+bn}{2b}\right) \cdot rect\left(\frac{x+bn}{b}\right) \\ &= \sum_n \int \cos\left(\frac{2\pi\alpha}{2b}\right) \cdot rect\left(\frac{\alpha}{b}\right) \delta(\alpha-(x+bn))\, d\alpha \\ &= \int \cos\left(\frac{2\pi\alpha}{2b}\right) \cdot rect\left(\frac{\alpha}{b}\right) \sum_n \delta(\alpha-(x+bn))\, d\alpha \qquad \text{(A.13)} \\ &= \int \cos\left(\frac{2\pi\alpha}{2b}\right) \cdot rect\left(\frac{\alpha}{b}\right) \left|\frac{1}{b}\right| comb\left(\frac{x-\alpha}{b}\right) d\alpha \\ &= \left[\cos\left(\frac{2\pi x}{2b}\right) \cdot rect\left(\frac{x}{b}\right)\right] * \left|\frac{1}{b}\right| comb\left(\frac{x}{b}\right) . \end{aligned}$$

The Fourier transform of the complete rectified cosine function may be simplified by using the identity

$$\mathcal{F}\{g(x) * h(x)\} = \mathcal{F}\{g(x)\} \cdot \mathcal{F}\{h(x)\}, \qquad \text{(A.14)}$$

by using the Fourier transform of the comb function

$$\mathcal{F}\left\{\left|\frac{1}{b}\right| comb\left(\frac{x}{b}\right)\right\} = \mathcal{F}\{comb(bf_x)\}, \qquad \text{(A.15)}$$

and by using the Fourier transform of a half period of the rectified cosine function derived above in Equation A.9.

The Fourier transform of the complete rectified cosine function simplifies to

$$\begin{aligned}\mathcal{F}\{t_2(x)\} &= \mathcal{F}\left\{\cos\left(\frac{2\pi x}{2b}\right)\cdot rect\left(\frac{x}{b}\right)\right\}\cdot\mathcal{F}\left\{\left|\frac{1}{b}\right|comb\left(\frac{x}{b}\right)\right\}\\ &= \frac{|b|}{2}\left[sinc\left(bf_x-\frac{1}{2}\right)+sinc\left(bf_x+\frac{1}{2}\right)\right]\cdot comb(bf_x)\\ &= \frac{1}{2}\left[sinc\left(bf_x-\frac{1}{2}\right)+sinc\left(bf_x+\frac{1}{2}\right)\right]\cdot\sum_{n=-\infty}^{\infty}\delta\left(f_x-\frac{n}{b}\right)\ .\end{aligned} \qquad \text{(A.16)}$$

The Fourier transform of the complete rectified sine function may be written as

$$\begin{aligned}\mathcal{F}\left\{\left|\sin\left(2\pi\frac{x}{2b}\right)\right|\right\} &= \mathcal{F}\left\{\left|\cos\left(2\pi\frac{x}{2b}-\frac{b}{2}\right)\right|\right\}\\ &= \mathcal{F}\left\{t_2\left(x-\frac{b}{2}\right)\right\}\ .\end{aligned} \qquad \text{(A.17)}$$

Using the identity

$$\mathcal{F}\{f(x-x_o)\} = e^{-j2\pi x_o f_x}\,\mathcal{F}\{f(x)\}, \qquad \text{(A.18)}$$

the Fourier transform of the complete rectified sine function simplifies to

$$\mathcal{F}\left\{\left|\sin\left(2\pi\frac{x}{2b}\right)\right|\right\} = e^{-j2\pi\frac{b}{2}f_x}\mathcal{F}\{t_2(x)\}\ . \qquad \text{(A.19)}$$

The electric field of the in-phase array mode in the near field (Equation A.1) may be rewritten as

$$E_{near}(x) = E_{near}(0)\cdot t_2\left(x-\frac{b}{2}\right)\cdot Gaus\left(\frac{x}{c}\right)\ . \qquad \text{(A.20)}$$

Making the same substitution in Equation A.3 yields the electric field in the far field.

$$\begin{aligned}E_{far}(f_x) &= \mathcal{F}\{E_{near}(x)\}\\ &= \mathcal{F}\left\{E_{near}(0)\cdot t_2\left(x-\frac{b}{2}\right)\cdot Gaus\left(\frac{x}{c}\right)\right\}\end{aligned} \qquad \text{(A.21)}$$

This may be simplified using the identity in Equation A.7, the Fourier transform of t_2 found in Equation A.16 and the Fourier transform of the Gaussian function.

$$\mathcal{F}\left\{Gaus\left(\frac{x}{c}\right)\right\} = |c|Gaus(cf_x) \qquad \text{(A.22)}$$

Thus the electric field in the far field becomes

$$\begin{aligned}
\frac{E_{far}(f_x)}{E_{near}(0)} &= \mathcal{F}\left\{t_2\left(x-\frac{b}{2}\right)\right\} \cdot \mathcal{F}\left\{Gaus\left(\frac{x}{c}\right)\right\} \\
&= \left\{e^{-j\pi bf_x}\frac{|b|}{2}\left[sinc\left(bf_x-\frac{1}{2}\right)+sinc\left(bf_x+\frac{1}{2}\right)\right] \cdot comb(bf_x)\right\} * |c|Gaus(cf_x) \\
&= \left\{e^{-j\pi bf_x}\frac{1}{2}\left[sinc\left(bf_x-\frac{1}{2}\right)+sinc\left(bf_x+\frac{1}{2}\right)\right] \cdot \sum_{n=-\infty}^{\infty}\delta\left(f_x-\frac{n}{b}\right)\right\} * |c|Gaus(cf_x) \\
&= \sum_n e^{-j\pi bn}\frac{1}{2}\int\left[sinc\left(b\alpha-\frac{1}{2}\right)+sinc\left(b\alpha+\frac{1}{2}\right)\right]\cdot\delta\left(\alpha-\frac{n}{b}\right)\cdot|c|Gaus(c(f_x-\alpha))d\alpha \\
&= \sum_n e^{-j\pi n}\frac{1}{2}\left[sinc\left(n-\frac{1}{2}\right)+sinc\left(n+\frac{1}{2}\right)\right] \cdot |c|Gaus\left(c\left(f_x-\frac{n}{b}\right)\right) \\
&= \sum_{n=-\infty}^{\infty}(-1)^n\ \frac{1}{2}\left[sinc\left(n-\frac{1}{2}\right)+sinc\left(n+\frac{1}{2}\right)\right] \cdot |c|Gaus\left(c\left(f_x-\frac{n}{b}\right)\right) \ .
\end{aligned}$$

(A.23)

Rewritten in terms of the electric field at the center of the far field this becomes

$$\frac{E_{far}(f_x)}{E_{far}(0)} = \frac{\sum_{n=-\infty}^{\infty}(-1)^n\left[sinc\left(n-\frac{1}{2}\right)+sinc\left(n+\frac{1}{2}\right)\right] \cdot Gaus\left(c\left(f_x-\frac{n}{b}\right)\right)}{\sum_{n=-\infty}^{\infty}(-1)^n\left[sinc\left(n-\frac{1}{2}\right)+sinc\left(n+\frac{1}{2}\right)\right] \cdot Gaus\left(\frac{c\,n}{b}\right)} \ . \qquad \text{(A.24)}$$

The associated intensity pattern is simply the square of the modulus of the electric field pattern.

$$\frac{I_{far}(f_x)}{I_{far}(0)} = \left[\frac{\sum_{n=-\infty}^{\infty}(-1)^n\left[sinc\left(n-\frac{1}{2}\right)+sinc\left(n+\frac{1}{2}\right)\right] \cdot Gaus\left(c\left(f_x-\frac{n}{b}\right)\right)}{\sum_{n=-\infty}^{\infty}(-1)^n\left[sinc\left(n-\frac{1}{2}\right)+sinc\left(n+\frac{1}{2}\right)\right] \cdot Gaus\left(\frac{c\,n}{b}\right)}\right]^2 \qquad \text{(A.25)}$$

A plot of this function is shown in Figure 3 of the main text for $b = \pi$, $c = 10$, and $n = -5, -4, -3 \ldots 3, 4, 5$.

The equation for the intensity pattern in the far field, for an array with an odd number of elements operating in the in-phase mode, is identical to Equation A.25 except it lacks the $(-1)^n$ coefficient.

APPENDIX B - Calculation of Far Field from Out-of-Phase Near Field

The electric field of the out-of-phase array mode, for an array with an even number of elements, may be written as (For an array mode with an odd number of elements replace the sine with a cosine)

$$E_{near}(x) = E_{near}(0) \cdot \sin\left(2\pi \frac{x}{2b}\right) \cdot Gaus\left(\frac{x}{c}\right), \qquad (B.1)$$

where

$$Gaus\left(\frac{x-x_o}{b}\right) = \exp\left[-\pi \left(\frac{x-x_o}{b}\right)^2\right], \qquad (B.2)$$

with
- x = Position coordinate along the horizontal axis in the near field,
- $2b$ = Distance between elements in the array,
- $2c$ = Approximate width of the array, and
- $E_{near}(0)$ = Electric field at the center of the array.

The electric field in the far field is given by the Fourier transform of the near field radiation pattern.

$$\begin{aligned} E_{far}(f_x) &= \mathcal{F}\{E_{near}(x)\} \\ &= \mathcal{F}\left\{E_{near}(0) \cdot \sin\left(2\pi \frac{x}{2b}\right) \cdot Gaus\left(\frac{x}{c}\right)\right\}, \end{aligned} \qquad (B.3)$$

where

$$f_x = \frac{x_f}{\lambda f}, \qquad (B.4)$$

with
- x_f = Position coordinate along the horizontal axis in the focal plane,
- λ = Wavelength, and
- f = Focal length.

This Fourier transform be simplified by using the identity

$$\mathcal{F}\{g(x) \cdot h(x)\} = \mathcal{F}\{g(x)\} * \mathcal{F}\{h(x)\} , \tag{B.5}$$

and by using the Fourier transforms of the sine and Gaussian functions

$$\mathcal{F}\left\{\sin\left(2\pi \frac{x}{2b}\right)\right\} = \frac{1}{2j}\left[\delta\left(f_x - \frac{1}{2b}\right) - \delta\left(f_x + \frac{1}{2b}\right)\right] , \tag{B.6}$$

$$\mathcal{F}\left\{Gaus\left(\frac{x}{c}\right)\right\} = |c| Gaus(cf_x) . \tag{B.7}$$

Thus the electric field in the far field becomes

$$\begin{aligned} \frac{E_{far}(f_x)}{E_{near}(0)} &= \mathcal{F}\left\{\sin\left(2\pi \frac{x}{2b}\right)\right\} \cdot \mathcal{F}\left\{ Gaus\left(\frac{x}{c}\right)\right\} \\ &= \frac{1}{2j}\left[\delta\left(f_x - \frac{1}{2b}\right) - \delta\left(f_x + \frac{1}{2b}\right)\right] \cdot * |c| \; Gaus(cf_x) \\ &= \frac{1}{2j} \int \left[\delta\left(\alpha - \frac{1}{2b}\right) - \delta\left(\alpha + \frac{1}{2b}\right)\right] \cdot |c| \; Gaus(c(f_x - \alpha)) d\alpha \\ &= \frac{|c|}{2j}\left[Gaus\left(c\left(f_x - \frac{1}{2b}\right)\right) - Gaus\left(c\left(f_x + \frac{1}{2b}\right)\right)\right] . \end{aligned} \tag{B.8}$$

Written in terms of the electric field at $f_x = 1/2b$ this becomes

$$\frac{E_{far}(f_x)}{E_{far}\left(\frac{1}{2b}\right)} = \left[\frac{Gaus\left(c\left(f_x - \frac{1}{2b}\right)\right) - Gaus\left(c\left(f_x + \frac{1}{2b}\right)\right)}{1 - Gaus\left(\frac{c}{b}\right)}\right] . \tag{B.9}$$

The associated intensity pattern is simply the square of the modulus of the electric field pattern.

$$\frac{I_{far}(f_x)}{I_{far}\left(\frac{1}{2b}\right)} = \left[\frac{Gaus\left(c\left(f_x - \frac{1}{2b}\right)\right) - Gaus\left(c\left(f_x + \frac{1}{2b}\right)\right)}{1 - Gaus\left(\frac{c}{b}\right)}\right]^2 \tag{B.10}$$

A plot of this function is shown in Figure 4 of the main text for $b = \pi$ and $c = 10$.

The equation for the intensity pattern in the far field, for an array with an odd number of elements operating in the out-of-phase mode, is identical to Equation B.9 except the two Gaussian functions are added instead of subtracted.

APPENDIX C - Calculation of SLM Far Field for Amplitude Modulation in Near Field

The SLM near field for amplitude modulation (no phase modulation) may be modeled as an infinite series of two-dimensional Rect functions.

$$E_{near}(x,y) = E_{near}(0,0) \cdot \sum_{n=-\infty}^{\infty} rect\left(\frac{x-an}{b}\right) \cdot \sum_{m=-\infty}^{\infty} rect\left(\frac{y-cm}{d}\right) , \quad (C.1)$$

where

$$rect\left(\frac{x-x_o}{b}\right) = \begin{cases} 0, & \left|\frac{x-x_o}{b}\right| > \frac{1}{2} \\ \frac{1}{2}, & \left|\frac{x-x_o}{b}\right| = \frac{1}{2} \\ 1, & \left|\frac{x-x_o}{b}\right| < \frac{1}{2} \end{cases} , \quad (C.2)$$

(For a sketch of rect(x) see Figure 12)

with
- x, y = Position coordinates along the horizontal and vertical axis in the plane of the modulator,
- b, d = Width, height of the high transmission bars, and
- a, c = Distance between bars.

The electric field in the far field is given by the Fourier transform of the near field radiation pattern.

$$\begin{aligned} E_{far}(f_x, f_y) &= \mathcal{F}\{E_{near}(x,y)\} \\ &= \mathcal{F}\left\{ E_{near}(0,0) \cdot \sum_{n=-\infty}^{\infty} rect\left(\frac{x-an}{b}\right) \cdot \sum_{m=-\infty}^{\infty} rect\left(\frac{y-cm}{d}\right) \right\} , \end{aligned} \quad (C.3)$$

where

$$f_x = \frac{x_f}{\lambda f} , \; f_y = \frac{y_f}{\lambda f} , \quad (C.4)$$

with
- x_f, y_f = Position coordinates along the horizontal and vertical axes in the focal plane,
- λ = Wavelength, and
- f = Focal length.

This is separable into two similar one dimensional equations.

$$E_{far}(f_x) = \mathcal{F}\{E_{near}(x)\} = \mathcal{F}\left\{E_{near}(0) \cdot \sum_{n=-\infty}^{\infty} rect\left(\frac{x-an}{b}\right)\right\} \qquad (C.5)$$

$$E_{far}(f_y) = \mathcal{F}\{E_{near}(y)\} = \mathcal{F}\left\{E_{near}(0) \cdot \sum_{m=-\infty}^{\infty} rect\left(\frac{y-cm}{d}\right)\right\} \qquad (C.6)$$

The analysis is simplified by calculating the result in one dimension and then using it in both dimensions. The electric field in the near field may be written as

$$\begin{aligned}\frac{E_{near}(x)}{E_{near}(0)} &= \sum_{n=-\infty}^{\infty} rect\left(\frac{x-an}{b}\right) \\ &= \sum_n \int rect\left(\frac{\alpha}{b}\right) \delta(\alpha-(x-an))\, d\alpha \\ &= \int rect\left(\frac{\alpha}{b}\right) \sum_n \delta(x-\alpha-an)\, d\alpha \\ &= \int rect\left(\frac{\alpha}{b}\right) \left|\frac{1}{a}\right| comb\left(\frac{x-\alpha}{a}\right) d\alpha \\ &= rect\left(\frac{x}{b}\right) * \left|\frac{1}{a}\right| comb\left(\frac{x}{a}\right) .\end{aligned} \qquad (C.7)$$

Using the identity

$$\mathcal{F}\{g(x) * h(x)\} = \mathcal{F}\{g(x)\} \cdot \mathcal{F}\{h(x)\} , \qquad (C.8)$$

and the Fourier transforms of the rect and the comb functions

$$\mathcal{F}\left\{rect\frac{x}{b}\right\} = |b|\ sinc\,(bf_x) , \qquad (C.9)$$

$$\mathcal{F}\left\{\frac{1}{|a|}\ comb\left(\frac{x}{a}\right)\right\} = comb(af_x) , \qquad (C.10)$$

the electric field in the far field may be written as

$$\begin{aligned}\frac{E_{far}(f_x)}{E_{near}(0)} &= \mathcal{F}\left\{rect\left(\frac{x}{b}\right)\right\} \cdot \mathcal{F}\left\{\left|\frac{1}{a}\right| comb\left(\frac{x}{a}\right)\right\} \\ &= |b|sinc(bf_x) \cdot comb(af_x) .\end{aligned} \qquad (C.11)$$

Rewritten in two dimensions in terms of the electric field at the center of the far field pattern this becomes

$$\frac{E_{far}(f_x, f_y)}{E_{far}(0,0)} = sinc(bf_x) \cdot comb(af_x) \cdot sinc(df_y) \cdot comb(cf_y) \ . \quad (C.12)$$

The intensity pattern in the far field is

$$\frac{I_{far}(f_x, f_y)}{I_{far}(0,0)} = \{sinc(bf_x) \cdot comb(af_x) \cdot sinc(df_y) \cdot comb(cf_y)\}^2 \ . \quad (C.13)$$

This corresponds well to the observed SLM far field intensity pattern as shown in Figure 13 of the main text.

APPENDIX D - Calculation of SLM Far Field for Amplitude Modulation and Phase Modulation in Near Field

The SLM near field, in one dimension, for amplitude and phase modulation may be modeled as an infinite series of rect functions times a phase modulation term.

$$E_{near}(x) = E_{near}(0) \cdot \left[rect\left(\frac{x}{b}\right) * \left|\frac{1}{a}\right| comb\left(\frac{x}{a}\right) \right] \cdot \exp\left[j\frac{m}{2}\sin(2\pi f_0 x) \right] \quad (D.1)$$

where
- x = Position coordinate along the horizontal axis in the plane of the modulator,
- b = Width of the high transmission bars,
- a = Distance between bars, and
- f_0 = The spatial frequency of the phase grating.

The electric field in the far field is given by the Fourier transform of the near field radiation pattern.

$$E_{far}(f_x) = \mathcal{F}\left\{ E_{near}(0) \cdot \left[rect\left(\frac{x}{b}\right) * \left|\frac{1}{a}\right| comb\left(\frac{x}{a}\right) \right] \cdot \exp\left[j\frac{m}{2}\sin(2\pi f_0 x) \right] \right\}, \quad (D.2)$$

where

$$f_x = \frac{x_f}{\lambda f}, \quad (D.3)$$

with
- x_f = Position coordinate along the horizontal axis in the focal plane,
- λ = Wavelength, and
- f = Focal length.

Using the identity

$$\mathcal{F}\{g(x) \cdot h(x)\} = \mathcal{F}\{g(x)\} * \mathcal{F}\{h(x)\}, \quad (D.4)$$

the Fourier transform of an infinite series of rect functions (calculated in Appendix C)

$$\mathcal{F}\left\{ \sum_{n=-\infty}^{\infty} rect\left(\frac{x-an}{b}\right) \right\} = |b|\, sinc(bf_x) \cdot comb(af_x), \quad (D.5)$$

and the Fourier transform for a sinusoidally varying phase grating

$$\mathcal{F}\left\{\exp\left[j\frac{m}{2}\sin(2\pi f_o x)\right]\right\} = \sum_{q=} J_q\left(\frac{m}{2}\right)\delta(f_x - qf_o) \ , \qquad (D.6)$$

the electric field in the far field may be written as

$$\begin{aligned}
\frac{E_{far}(f_x)}{E_{near}(0)} &= \mathcal{F}\left\{rect\left(\frac{x}{b}\right) * \left|\frac{1}{a}\right| comb\left(\frac{x}{a}\right)\right\} * \mathcal{F}\left\{\exp\left[j\frac{m}{2}\sin(2\pi f_0 x)\right]\right\} \\
&= [b\ sinc(bf_x) \cdot comb(af_x)] * \mathcal{F}\left\{\sum_{q=-\infty}^{\infty} J_q\left(\frac{m}{2}\right)\exp(j2\pi q f_0 x)\right\} \\
&= [b\ sinc(bf_x) \cdot comb\ (af_x)] * \left[\sum_q J_q\left(\frac{m}{2}\right)\delta(f_x - qf_0)\right] \\
&= \int b\ sinc(b\alpha) \cdot comb\ (a\alpha) \cdot \sum_q J_q\left(\frac{m}{2}\right)\delta(f_x - qf_o - \alpha)\, d\alpha \\
&= \sum_q J_q\left(\frac{m}{2}\right) \int b\ sinc(b\alpha) \cdot comb\ (a\alpha) \cdot \delta(f_x - qf_0 - \alpha)\, d\alpha \\
&= \sum_{q=-\infty}^{\infty} J_q\left(\frac{m}{2}\right) b\ sinc[b(f_x - qf_0)] \cdot comb\ (a(f_x - qf_0)) \ .
\end{aligned} \qquad (D.7)$$

The intensity pattern in the far field is

$$\frac{I_{far}(f_x)}{I_{near}(0)} = \left\{\sum_{q=-\infty}^{\infty} J_q\left(\frac{m}{2}\right) b\ sinc[b(f_x - qf_0)] \cdot comb\ (a(f_x - qf_0))\right\}^2 \ . \qquad (D.8)$$

This corresponds well to the observed SLM far field intensity pattern as shown in Figure 21 of the main text.

VITA

Captain Gregory S. Kenyon was born on 11 October 1964 in Honolulu, Hawaii. In 1971 his family moved to Dallas, Oregon where he graduated from Dallas High School in 1983. He attended Oregon State University, graduating with Bachelor of Science degrees in Physics and Engineering Physics in June 1988. Upon graduation, he received a reserve commission in the USAF and served his first tour of duty at Kirtland AFB, New Mexico. He was the lead analyst on the Airborne Self Protection Jammer (ASPJ), Tacit Rainbow anti-radiation missile, and the High-Speed Anti-Radiation Missile (HARM) for the Air Force Operational Test and Evaluation Center (AFOTEC). In May of 1992 he entered the School of Engineering, Air Force Institute of Technology where he will graduate in December of 1993 with a Master of Science in Engineering Physics. His follow on assignment is to the Star Fire Optical Range at Kirtland AFB.

Permanent Address: 16840 Oakdale Road
Dallas, OR 97338

REPORT DOCUMENTATION PAGE

Form Approved
OMB No. 0704-0188

1. AGENCY USE ONLY (Leave blank)	2. REPORT DATE	3. REPORT TYPE AND DATES COVERED
	December 1993	Master's Thesis

4. TITLE AND SUBTITLE
CHARACTERIZATION OF AN LCD FOR USE AS A PROGRAMMABLE PHASE SHIFTER TO PRODUCE A SINGLE-LOBED FAR-FIELD PATTERN IN A PHASED ARRAY

5. FUNDING NUMBERS

6. AUTHOR(S)
Gregory S. Kenyon, Captain, USAF

7. PERFORMING ORGANIZATION NAME(S) AND ADDRESS(ES)
Air Force Institute of Technology, WPAFB OH 45433-6583

8. PERFORMING ORGANIZATION REPORT NUMBER
AFIT/GAP/ENP/93D-05

9. SPONSORING/MONITORING AGENCY NAME(S) AND ADDRESS(ES)
Dr. Christopher Clayton
PL/LIDN, KAFB NM

10. SPONSORING/MONITORING AGENCY REPORT NUMBER

11. SUPPLEMENTARY NOTES

12a. DISTRIBUTION/AVAILABILITY STATEMENT
Approved for public release; distribution unlimited

12b. DISTRIBUTION CODE

13. ABSTRACT (Maximum 200 words)

The liquid crystal display (LCD) from an inexpensive pocket television was converted to a spatial light modulator (SLM) for the purpose of altering the phase front of a ten element diode laser array to produce a single lobe far field pattern. Characterization of the SLM determined the amount of phase shift, amplitude modulation and polarization rotation properties. Nonuniformities within the phase shifter and insufficient phase shift prevented the formation of a single lobe. However, a very limited phase grating was created and analyzed. LCDs from inexpensive commercial pocket televisions were found unsuitable for use as phase shifting spatial light modulators.

14. SUBJECT TERMS	15. NUMBER OF PAGES
Semiconductor Lasers, Liquid Crystal Display Systems, Infrared Lasers, Laser Applications	69
	16. PRICE CODE

17. SECURITY CLASSIFICATION OF REPORT	18. SECURITY CLASSIFICATION OF THIS PAGE	19. SECURITY CLASSIFICATION OF ABSTRACT	20. LIMITATION OF ABSTRACT
Unclassified	Unclassified	Unclassified	UL